EFFECT OF AQUEOUS ENVIRONMENTS ON THE FATIGUE BEHAVIOUR OF 90-10 COPPER NICKEL

by

Daniel P. Harvey, II

Thesis submitted to the Faculty of
Virginia Polytechnic Institute and State University
in partial fulfillment of the requirements for the degree
of

MASTER OF SCIENCE

in

Materials Engineering

APPROVED:

M. R. Louthan, Jr., Chairman

N. E. Dowling

W. R. Hibbard

August, 1985

Blacksburg, Virginia

EFFECTS OF AQUEOUS ENVIRONMENTS ON THE FATIGUE BEHAVIOR OF 90-10 COPPER NICKEL

by

Daniel P. Harvey, II

ABSTRACT

Fatigue tests on compact tension specimens of 90-10 copper nickel were conducted in 3.5% NaCl solutions. Anodic or cathodic currents were applied during testing. Anodic currents decreased and cathodic currents increased the fatigue life. Both anodic and cathodic currents changed the fracture mode from predominantly transgranular to intergranular. Constant extension rate tests were performed on similar CT specimens in environments of 3.5% NaCl solution and 3.5% NaCl solution titrated to pH 1.0 with various levels of applied current. The environment had little influence on the monotonic failure of 90-10 copper nickel. Polarization studies were conducted to determine the effects of welding and pH on the corrosion behavior of 90-10 copper nickel. The rate of corrosion was less in the weld and the heat affected zone than in the base metal. As the pH of the

environment was lowered, the corrosion rate of 90-10 copper nickel increased due to the retardation of film formation and repassivation.

These studies showed that three different mechanisms of corrosion fatigue were likely: localized anodic dissolution, surface film rupture and hydrogen embrittlement. The dominance of one mechanism over the other two depends on the applied current. No evidence of susceptibility to stress corrosion cracking was found, therefore, a true corrosion fatigue process is operative in 90-10 copper nickel.

ACKNOWLEDGEMENTS

The author wishes to express his gratitude to Dr. M. R. Louthan, Jr. for the guidance and encouragement given throughout this project. The contributions of Dr. W. R. Hibbard and Dr. N. E. Dowling are also appreciated. Thanks must also go the Dr. T. S. Sudarshan for pushing the author from time to time in order to prevent inertia from setting in. The author wishes to thank for the typing of this manuscript. The author also wishes to thank his fellow graduate students for maintaining an above average level of levity in the graduate office and all of the Materials Engineering secretaries who never failed to brighten his day. Finally, the author wishes to thank his parents, and the rest of his family for their love, support and especially their prayers which have sustained the author through both easy and difficult times.

TABLE OF CONTENTS

LIST OF FIGURES

LIST OF TABLES

INTRODUCTION

A major expense involved in the operation of an ocean going vessel is the degradation of the steel ship hull due to general corrosion, biofouling and erosion-corrosion. This expense is accrued in a number of ways. Steel hull degradation from biofouling and corrosion causes a substantial increase in the surface roughness of the hull. Surface roughness can cause a 15 to 20 percent increase in drag which causes a substantial increase in power requirements and therefore leads to an increase in fuel and transportation costs. Degradation of the hull also leads to maintenance costs which include drydocking and cleaning. In addition, such drydocking leads directly to lost revenues because the ship is out of service for maintenance.

Costs due to the degradation of steel ship hulls have led to the consideration of the use of copper alloys as hull cladding materials. Copper and copper alloys have been used extensively in the marine industry as piping for condensers, heat exchangers and distillation plants because of their general corrosion resistance in salt water environments. These alloys, when immersed in sea water, discharge a constant low level of copper ions which act as a poison to marine

organisms. This poisoning prevents biofouling and therefore significantly decreases the need for drydocking. This combination of properties causes the alloys to be considered for cladding not only for ship hulls but for off-shore oil drilling platforms and ocean thermal energy conversion systems.

One of the primary alloys under consideration is 90-10 copper nickel. This alloy is being considered because of its superior mechanical properties when compared to pure copper and because of its excellent erosion-corrosion resistance due to the addition of small amounts (0.5 to 1.5 percent) of iron. Previous studies (1) have determined that the presence of a small amount of iron in the copper-nickel matrix is beneficial to the corrosion resistance. Investigators (2) have also shown that for improved corrosion resistance, the presence of iron in solution was far more beneficial than iron in the form of second-phase particles. However, in commercially produced copper-nickel alloys, the iron tends to precipitate in an almost pure form. These precipitate particles are distributed both in the matrix and along the grain boundaries.

There are a number of processes that may be used to attach the copper-nickel cladding to the steel hull. The copper-nickel may be metallurgically attached to the

steel by roll-bonding the two layers. This method of attachment has been used successfully in the construction of shrimp boats (3); however, roll-bonding has a major disadvantage in that it can only be used in new construction. An alternative to roll-bonding is to have a loose copper-nickel cladding over the steel hull with the cladding attached only at selected places. A major advantage of this technique is that the copper-nickel plates can be attached to steel structures which have already been fabricated.

In the loose cladding method, there are a number of alternatives as to how to attach the copper-nickel to the steel including gluing and welding. In the gluing process, an adhesive is placed between the copper-nickel cladding and steel structural component. Gluing offers the advantage of placing a non-conductive barrier between the copper-nickel and the steel. Such a barrier minimizes the possibility of galvanic cell generation between the two dissimilar metals. Unfortunately, gluing doesn't provide sufficient bonding strength, especially under conditions where sea water flows across the cladding at high velocities. This disadvantage can be overcome by welding. At least three types of welding have been considered: resistance spot welding, ultrasonic welding and submerged metal arc welding. However,

submerged metal arc welding appears to be the best in terms of structural integrity (4). In this technique, welds are used to attach individual copper-nickel sheets about their periphery to the steel hull with supplemental interior welds to reduce the buckling of the sheets during loading. A disadvantage of welding, however, is that this attachment technique causes dissimilar metals to be in electrical contact while exposed to marine environments. This contact allows the generation of local galvanic corrosion cells which can influence the behavior of both the steel and the copper-nickel. The possibility for local corrosion cells coupled with the buckling and flexing of the copper-nickel cladding sheets due to the action of waves against the ship hull can lead to conditions which will cause the generation of corrosion fatigue cracks in the copper-nickel cladding.

The purpose of this research is to study the effects of aqueous environments on the fatigue behavior of 90/10 copper-nickel. Experiments were performed in order to determine the effects of various aqueous environments on the fatigue life as well as to determine the mechanisms of crack growth in the 90 Copper-10 Nickel alloy.

LITERATURE REVIEW

The subject of fatigue has been studied extensively by several researchers but a great deal of disagreement still exists among the various models and mechanisms which describe this process. The subject has been broadly divided into two categories; namely, a) fatigue crack nucleation and b) fatigue crack propagation. Most of the research in recent years has focused on the general area of fatigue crack propagation because it is assumed by designers that cracking, flaws, defects or discontinuities are inherently present in any engineering structure. Early research on fatigue, particularly that which was conducted in the academic environment, failed to separate the process into the two separate categories of crack nucleation and crack propagation and thus there is very little attention that has been focused exclusively on the area of fatigue crack nucleation. Environmental effects complicate the response of a material to fatigue and has been an area of considerable interest in a wide variety of metal alloy systems. In this review several of the fatigue crack nucleation models will be highlighted and some of the anomalies will be discussed from results available in the open literature with subsequent emphasis on environmental

effects on crack nucleation. Subsequently, models proposed for crack growth along with environmental effects will be discussed. Although environmental effects on fatigue have been studied in a wide range of both gaseous and aqueous environments, this literature review will focus only on fatigue behavior in aqueous environments.

Fatigue Crack Nucleation

Over the years, research in the area of fatigue has led to several hypotheses for fatigue crack nucleation. Most investigators generally agree that nucleation occurs from the surface although sub-surface nucleation (5,6) has also been reported. This sub-surface nucleation has been observed in metals with a strong adherent metal surface oxide which retards the nucleation at the external surface. A number of models for fatigue crack nucleation have been proposed and can be generally classified into:

1) single slip-system models,
2) alternating parallel slip system models and,
3) two intersecting slip line models.

Each of these models will be described and discussed below.

Models For Fatigue Crack Nucleation

One of the earliest models (7, 8, 9) proposed was associated with intrusions which were formed by the repeated slip of layers of atoms on a single slip system. This process is schematically illustrated in Figure 2.1. After the intrusion is initially formed it acts as a stress raiser and facilitates further slip only at the notch root.

Another (10) model of crack nucleation was also based on the idea of slip due to repeated stresses. However, this model involved the formation of cracks by coarse slip on alternating parallel slip planes (Figure 2.2). In this model, the initial deformation is due to slip along slip plane 1. The excess dislocations of one sign remain on this slip plane. The first slip step produced then acts as a stress raiser which leads to the activation of slip plane 2. This causes configuration (b) and the generation of excess dislocations on plane 2. When compressive loading occurs, the excess dislocations on planes 1 and 2 run back which leads to the crack nucleus shown in (c). As this process is repeated on other glide planes of the same slip systems, the length of the microcrack is increased.

Other models (11) have been proposed for crack nucleation involving more than one slip system. Two

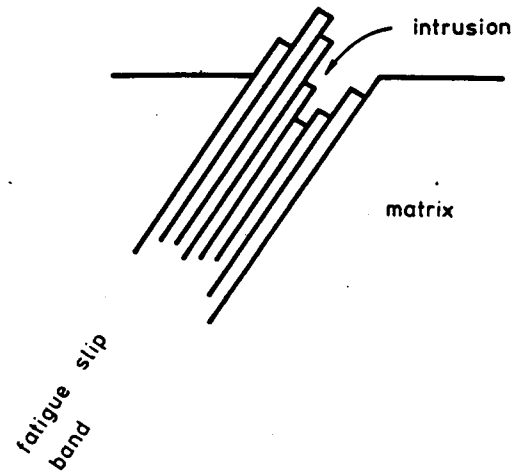

Figure 2.1 Single slip system model of intrusion formation.

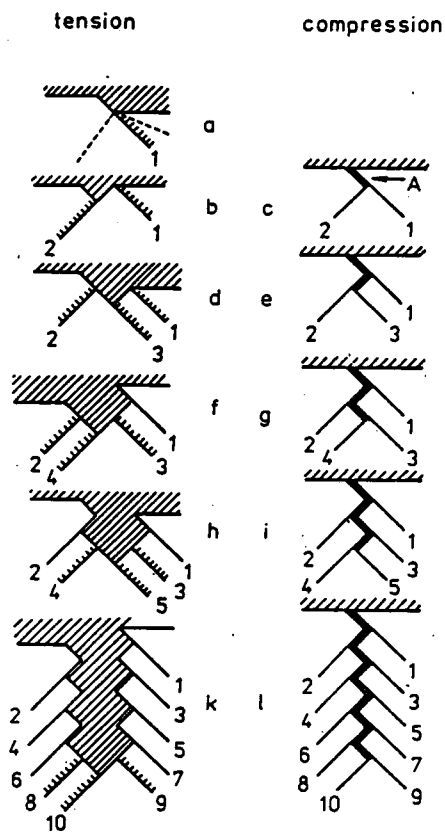

Figure 2.2 Neumann's model of crack nucleation.

intersecting slip bands may operate sequentially during both the tension and compression halves of the stress cycle. This model is illustrated in Figure 2.3.

The preceding crack nucleation models are rather attractive for ductile materials which have an abundant availability of slip systems due to their very general nature. None of the models require any specific slip systems nor any specific dislocation interactions. These models are therefore preferable to other models which require specific conditions to be operable. The models involving repeated slip cannot, however, satisfactorily explain the crack nucleation behavior in brittle materials. Such materials could include dispersion strengthened composites, high yield strength steels or materials containing brittle second phase particles. Similarly, a model which requires the condensation of vacancies requires the presence of high temperatures and therefore cannot serve as a general explanation for crack nucleation. Other models involving the nucleation of cracks in grain boundaries require polycrystalline samples. Such requirements are not always met. For example, fatigue occurs in single crystals therefore the grain boundary nucleation model cannot be accepted as a generalized model for fatigue.

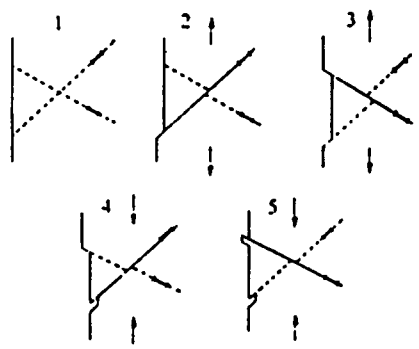

Figure 2.3 Cottrell and Hull's model for intrusion Formation.

Environmental Effects on Crack Nucleation

Little attention has been focused on the effects of an aggressive aqueous environment on fatigue crack nucleation. It is generally agreed among the few researchers who have studied this topic that the presence of an aggressive aqueous environment typically reduces the fatigue life of metallic specimens. While initiation of fatigue cracks in smooth polished specimens fatigued in air may occupy as high at 90% of the total fatigue life, the percentage of total life required for nucleation in aggressive aqueous environments can be reduced to as little as 10%. Contact with an aggressive environment probably has the same effect on fatigue life as the machining of a sharp notch into the surface. A stress raiser develops and fatigue cracks grow. It may be surmised that a corrosive environment therefore simply facilitates the formation of geometric discontinuities in the surface of metal specimens. These discontinuities then become fatigue cracks during cyclic loading.

Several mechanisms have been proposed for environmental effects on fatigue crack nucleation. These mechanisms include:

1) formation of corrosion pits
2) surface film rupture
3) strain inhanced dissolution of slip steps and

4) lowering of surface energy due to adsorption of a specific species from the environment.

All mechanisms that have been proposed involve a synergistic contribution from mechanical and chemical parameters. While some of the mechanisms require a dominance of the mechanical aspects, other mechanisms are influenced by the chemical aspects of the phenomenon. Each of these mechanisms is described below and discussed in light of available experimental data.

Mechanism of Pitting in Aqueous Environments

Early work by investigators (12, 13) indicated that a corrosive media can assist the nucleation of fatigue cracks by the formation of corrosion pits on the metal surface. This was clearly demonstrated through prepitting by corrosion exposures with subsequent fatigue testing in air. Such prepitting reduced the air fatigue life. However, prepitting then testing in the same corrosive environment reduced the fatigue life even further. Thus environmental effects must extend beyond the initiation process. Metallographic examination of the failed specimens revealed that in fact a number of large cracks originated at large hemispherical corrosion pits on the metal surface. However, subsequent studies (14, 15) showed that the formation of corrosion pits is not essential for easier crack nucleation. For instance,

corrosion fatigue was observed in low carbon steels tested in acid solutions which did not cause pit formation on the steel surfaces. Reduced fatigue lives were also observed in steel specimens tested while a small anodic current was applied to the sample. When tests were conducted in deaerated solutions, pits did not form but the fatigue life decreased. Steels which were tested in 3% NaCl solutions (16) and metallographically examined showed that pits formed by preferential corrosion of already existing intrusions. No cracks, however, eminated from these pits. It was then concluded in this case that the pits were not the cause of corrosion fatigue but perhaps the result of corrosion after the fatigue crack was initiated. This is not totally unexpected because corrosion induced pits tend to have hemispherical geometries and the stress intensity associated with hemispherical surface defects is not very high (17). Another factor which the prepitting mechanism does not satisfactorily explain is the initiation of cracks in the absence of gravity effects. In normal pitting processes, gravity plays a major role in determining the shape, size and severity of the pit. Further, the pitting mechanism depends strongly on the chemical contributions which may not necessarily be dominating in a corrosion fatigue process. Thus, the

prepitting mechanism failed to comprehensively explain the synergistic contribution that is necessary to initiate cracks during the process of corrosion fatigue.

Mechanism of Surface Film Rupture for Crack Initiation

Another mechanism that has been proposed to explain initiation during corrosion fatigue is the rupture of protective surface films. An important step in this mechanism is the formation of the protective surface film. Such films are generally formed by materials which have a high affinity for oxygen, which is readily available in aqueous environments. Thus film formation involves a chemical reaction which dominates the mechanism of corrosion fatigue before mechanical parameters can participate in the initiation process. Prior to film formation, both anodic and cathodic corrosion reaction sites exist on the surface of a metal in an aqueous solution. The formation of a protective film shields these sites from the environment and thus prevents corrosive attack from taking place. However, when the protective film is subjected to mechanical stressing, the film is broken which exposes fresh metal which may then act as an anodic or cathodic reaction site.

The rate of formation of a protective surface film

on any material is strongly influenced by the nature of the aggressive environment to which it is exposed. Aggressive environments can be:

a) acidic in nature (pH<7)

b) neutral solutions (pH=7) or

c) basic solutions (pH>7).

Each one of these categories of solutions significantly influences the chemical contribution to the mechanism of corrosion fatigue crack nucleation.

The observation has been made that corrosion fatigue occurs in acidic solutions where adherent protective surface films are unstable. This observation was interpreted to suggest that film rupture cannot be accepted as a general mechanism for corrosion fatigue and led to the suggestion (14) that film rupture may be important in neutral solutions but that strain enhanced dissolution could be involved in acidic solutions. However, the observation that adherent films are unstable in acidic solutions might also suggest that the formation of the protective surface film under these conditions was an extrememly rapid process and the films probably reached a critical thickness and spalled off before mechanical parameters could influence the crack initiation mechanism.

Effects of pH on crack nucleation have been

observed in aluminum exposed to NaCl solutions (18). This effect has been attributed to the stability of aluminum oxide films since the solubility of Al_2O_3 varies with pH. At low pH's, the solubility of Al_2O_3 is rather high and consequently film formation is difficult. At pH7, $Al_2O_3$is relatively insoluble and so the initial oxide film will protect the underlying metal until the film is mechanically disturbed. At pH10 the solubility of Al_2O_3 is again increased so that lateral dissolution is less restricted and crack blunting is induced.

The corrosion fatigue of drawn mild steel wires exposed to KCl solutions with and without K_2CrO additions showed that the measured electrode potential dropped suddenly when loading took place (19). These drops in potential occurred several times during the fatigue tests and were interpreted to indicate a breakdown of a protective film.

Other investigators disagree strongly with the surface film rupture mechanism because experimental data on low carbon steel exposed to chloride solutions (20) have shown that there appears to be a critical corrosion rate necessary for initiating corrosion fatigue which was observed to be independent of the applied stress level. However, it is not clear from these studies if the mechanical parameters were sufficient to dominate the

crack initiation mechanism. It may very well be that a critical applied stress in combination with the critical corrosion rate promotes the surface film rupture mechanism of crack initiation.

Mechanism of Strain Induced Dissolution for Crack Initiation

A third model that has been proposed by investigators is based on strain enhanced dissolution of emerging slip bands. A series of corrosion fatigue experiments performed on cold worked and annealed steel wires showed that cracks advanced by a combination of electrochemical and mechanical action (21). The preferential attack of the slip bands accelerates further slip in an autocatalytic process. Evidence for such a mechanism has been shown in mild steels and copper alloys (19, 22, 23). The preferential attack of slip bands is explained through the higher energy state of metal atoms associated with dislocations when compared to metal atoms in a lattice. The atoms associated with dislocations are preferentially attacked because it takes less activation energy to remove these atoms from the material.

Experiments performed on polycrystalline pure copper showed that if anodic currents were applied, the fatigue fracture morphology changed from transgranular-intergranular to totally intergranular (24). This behavior

has been thought to suggest that the enhanced deformation associated with grain boundaries causes increased corrosive attack of the grain boundaries relative to that of emerging slip bands.

In all of the experiments performed to support the hypothesis of strain-enhanced dissolution the materials were in an environment which allowed the formation of protective surface films. This fact was, for the most part, ignored by the investigators. The fact that film formation took place could explain why preferential corrosion occured at emerging slip bands because it would be at these emerging slip bands where film rupture would occur.

Mechanism of Surface Adsorption for Crack Nucleation

One final mechanism proposed for crack nucleation involves the lowering of the surface energy of a metal due to adsorption of specific species from the environment. Such species adsorption lowers the local bond energies and promotes crack formation. Some investigators have also suggested that reductions in surface energy may enhance plasticity and early crack initiation (25). An alternate view of the above suggestion is that adsorption reduces plasticity and allows nucleation of cracks due to local brittle failure (26). Such conclusions were strengthened through

experiments on Al-Zn-Mg alloys exposed to water which exhibited totally brittle fracture. Since hydrogen was the only stable gaseous species present, failure can be attributed to hydrogen embrittlement because there is no sign of anodic dissolution or plasticity (27). However, the authors ignored the fact that surface films were present and could also contribute to the initiation process.

From a review of the above mechanisms, it is clear that the most promising approach to explaining several of the observed results is the mechanism of surface film rupture, particularly under conditions of anodic polarization. Most investigators ignore the ability of a metal to form a protective film when exposed to aqueous environments. Unless careful attention is paid in all future corrosion fatigue experiments to the nature and rate of formation of a surface film, seemingly contradictory mechanisms will continue to be proposed. It is the belief of the author that corrosion processes dominate the initial stages of nucleation and subsequent stages of nucleation are controlled by mechanical parameters.

Fatigue Crack Propagation

Most current models of fatigue crack propagation in ductile materials agree in all but the more trivial

aspects of the model. These models are based mainly on trying to explain the striations observed on the fracture surface of fatigued specimens and on the direct observation of fatigue crack tip behavior in the scanning electron microscope. All the fatigue models depend on the fact that the fatigue process is repetitive in nature and therefore the models try to develop the crack propagation mechanism by explaining the processes that takes place during one loading cycle.

One of the earlier mechanisms for fatigue crack propagation (28) demonstrates, through a series of fatigue tests, that each fatigue striation was associated with a single stress cycle. This model assumes that the flat region of the fracture surface between each striation was caused by cleavage fracture occurring ahead of the crack tip and that each elevated striation was formed by ductile necking at the crack tip.

This mechanism of brittle-ductile fracture was later refuted through direct observations made of crack tip processes (29, 30). These direct observations were made by sectioning specimens which had been strain cycled until they were known to contain cracks and were unloaded at various points on the tension and compression portions of the stress cycles (31). The mechanism proposed from these observations is known as the "plastic blunting

process" and is a process which is comprised totally of ductile fracture mechanisms. This mechanism is illustrated in Figure 2.4. Figure 2.4(a) represents a well developed Stage II fatigue crack which exhibits striations on the fracture surface. As a small tensile load is applied (b), the metal begins to plastically yield. This deformation occurs mainly along slip planes at 45^{o} from the stress axis. As the maximum tensile load is reached (c), the crack tip radius increases and the crack tip blunts to a semi-circular configuration. As the compressive load is applied (d), the direction of slip in the slip zones reverses and the distance between the matching surfaces decreases. However, the new surface created in tensile loading cannot be completely removed by rejoining of atomic bonds. This new surface is partially folded by buckling into a double notch at the tip. The final configuration at the maximum compressive load (e) is once again a sharp crack tip; however, the crack length has been increased by a length equal to the spacing between the previous and the new striations. As the tensile load is increased again (f), the process is repeated.

This plastic blunting model is widely accepted as a general description of fatigue crack propagation. However, there is some disagreement as to how this

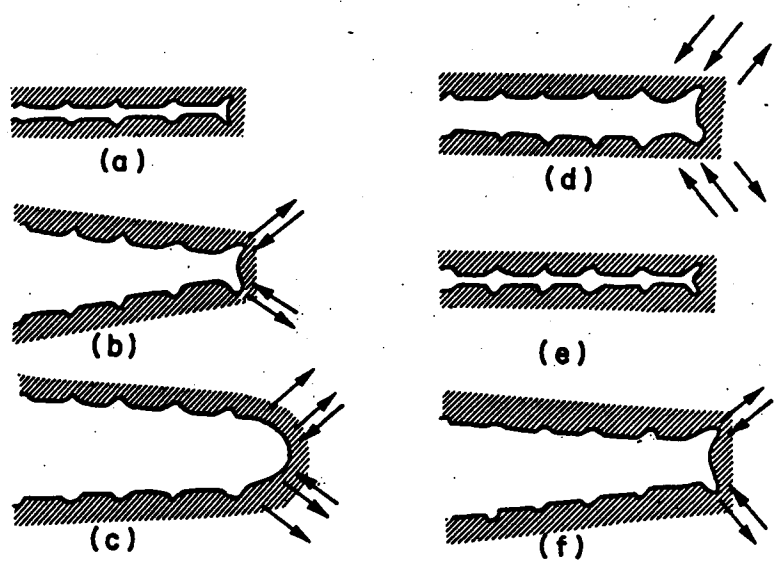

Figure 2.4 Laird's "Plastic Blunting Process" of fatigue crack propagation.

plastic blunting actually occurs. Many studies have demonstrated that fatigue crack propagation can occur by slip on alternating sets of slip planes. This mechanism was first observed in an aluminum alloy (7075-T6) through fractographic and etch pit studies (32). Later studies on silicon-iron and copper confirmed this mechanism through observations made at the crack tip of specimens that were cyclically loaded while being observed in a scanning electron microscope (33, 34). A schematic of this mechanism is shown in Figure 2.5.

A variant of the alternating slip plane model is the unzipping model (35). Again, in this model, slip occurs on alternating slip planes. As the applied stress increases, Figure 2.6 shear takes place alternately on slip bands 1, 2, 3 and 4 in succession. The slabs of material between the slip planes move away from the crack tip one at a time. As the slabs move, the crack front progresses forward. One of the major differences between the unzipping model and the other alternating slip plane models is that in the unzipping model, not all of the plastic deformation goes into advancing the crack front.

A mechanism for fatigue crack propagation which involved tensile tearing as well as shear slip has also been proposed (36). In fractographic studies of fatigued samples of annealed aluminum, it was found that a large

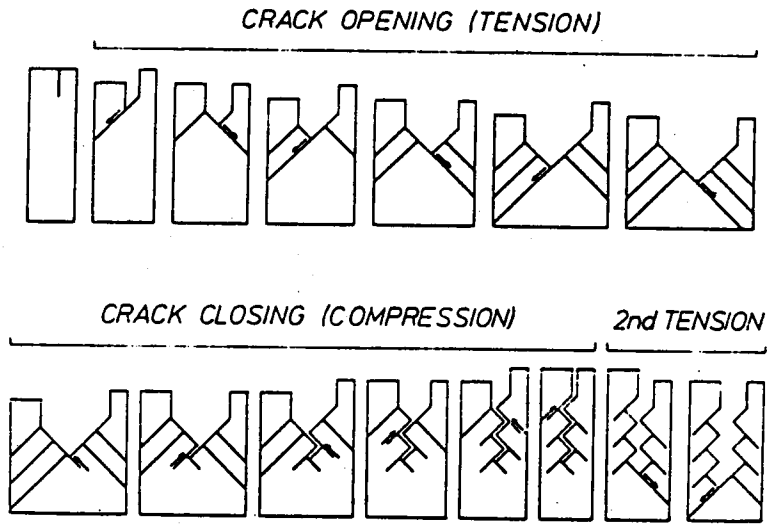

Figure 2.5 Coarse slip model of fatigue crack propagation.

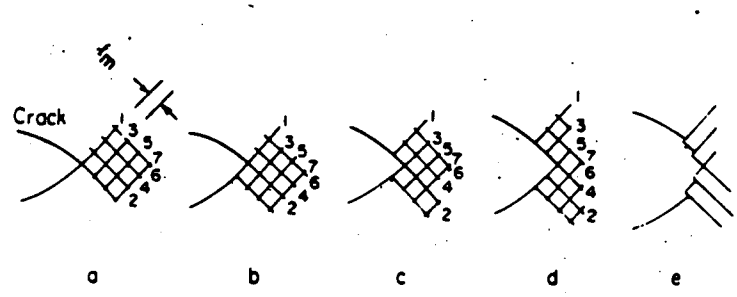

Figure 2.6 The "unzipping" model for fatigue crack propagation.

striation was was succeeded by a number of finer ripples at high strains. Support for this observation was made on fracture surfaces of fatigued aluminum alloys 2024-T3 and 7075-T6 (37). This tearing-shearing model is shown in Figure 2.7. At the maximum compressive load the crack tip is sharp. As a tensile load is applied, plastic flow occurs along well defined slip planes. A new crack surface is formed and a blunted crack tip is produced. Under continued tensile loading, this shear deformation is stopped on the original slip planes because of considerable strain hardening. Fracture by tensile tearing then occurs at the center of the blunted crack tip which then allows further blunting on new slip planes. This process continues until the maximum tensile stress is reached. When the compressive load is applied, the slip direction reverses on the slip planes which results in striations. All of the above models are specifically for metals and involve the concept of plasticity. Until an understanding of the other parameters that affect plasticity is developed, these models will be the best suited to explain fatigue crack propagation.

Environmental Effects on Crack Propagation

It is generally accepted that when a material is exposed to an aggressive environment, its fatigue crack

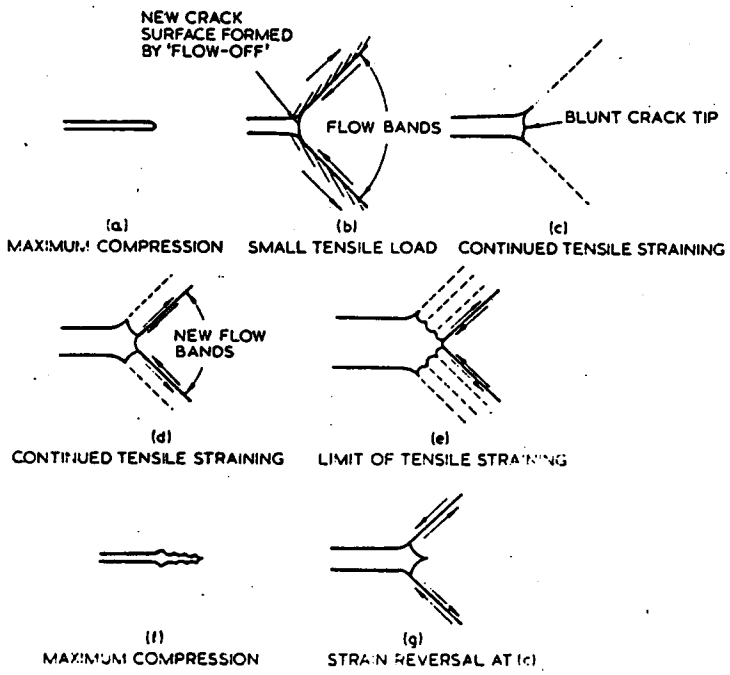

Figure 2.7 Tearing and shearing model of fatigue striation formation.

growth rate will increase. The only exceptions found to this generality were two studies (38, 39) in which structural steels were exposed to extreme conditions and the crack growth rate decelerated due to corrosion products wedging the crack tip. However, accelerated crack growth rates due to environmental interaction have been seen in a number of systems including steels (40-43) aluminum alloys (44-46), copper based alloys (22-24), and titanium alloys (47-49). There are a number of mechanisms that explain accelerated fatigue crack growth due to environmental effects. These mechanisms include:

1) preferential electrochemical attack of plastically deformed metal,
2) rupture of protective surface films and
3) surface energy reduction due to absorption of aggressive chemical species.

These mechanisms are presented and discussed below.

Mechanism of Preferential Attack of Plastically Deformed Material

The mechanism of preferential electrochemical attack of plastically deformed areas of metals, where the non-deformed metal acts as a cathode, has been put forth in several studies (15, 20-24, 50, 51). As new slip bands emerge near a fatigue crack tip, the slip bands are preferentially attacked by the aggressive environment.

This attack is due to interactions between the environment and metal atoms associated with the highly strained regions near dislocations (22). Such atoms may be more susceptible to corrosive attack because the total bond strength of atoms associated with dislocations will be less than that of atoms in a normal lattice. In addition to the strain, the vacancy concentration associated with the dislocation may also promote the localized attack.

Experiments were conducted (52) to find a correlation between loading and the dissolution rate of a fatigue specimen subjected to an aggressive environment. It was found that for both mild steel and stainless steels when the maximum tensile or compressive load was applied in each stress cycle, peaks in the dissolution rate occurred. A typical dissolution transient is shown in Figure 2.8. The peaks in dissolution rate were attributed to the slip step motion which occurred at the loading peaks.

This mechanism of preferential attack of plastically deformed metal is operative only in the active region of a polarization curve. In this region, no effects due to film formation or cathodic reactions are significant. If the metal-environment interaction is such that the metal is in the passive or immune region of the polarization

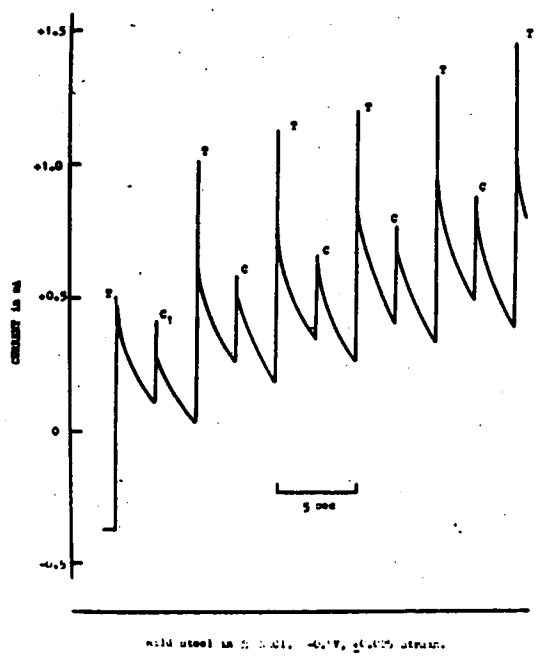

Figure 2.8 Typical dissolution transient for mild steel in 3% NaCl solution.

curve, then some other crack propagation mechanism is operative.

Mechanism of Surface Film Rupture

A second mechanism for accelerated fatigue crack growth in an aggressive environment is preferential corrosive attack at ruptures in an otherwise protective surface film. This process has been observed mainly to stainless steels and aluminum alloys (51, 53-58) whose natural corrosion potentials in neutral sea water lie in the passive region. As slip bands emerge or as the crack opening displacement increases due to tensile loading, ruptures in a protective surface film will provide areas of bare metal where anodic dissolution can occur. Evidence for such a mechanism has been observed in several studies. Fatigue tests were conducted on four different stainless steels in an aqueous solution containing sodium chloride. The results showed that the stainless steel with the highest chromium content, and therefore the highest repassivation rate, had the smallest decrease in fatigue life when placed in the aqueous environment. It was also found that at low loads, oscillations in potential could be correlated with cycles of depassivation and repassivation. Fatigue tests (59) conducted on an austenitic-ferritic stainless steel in aqueous solutions of various pH's showed that as

the pH of the solution got progressively lower, the protective films were broken down and eventually removed. As the films were removed, a corresponding increase in the fatigue crack growth rate was observed. Specimens of a 13% chromium steel were fatigued (60) in aqueous solutions containing progressively higher contents of Cl^-, a chemical species known to promote pitting in stainless steels. As the chloride content was increased, the fatigue crack growth rate of the steel was increased due to increased damage in the protective chromium oxide surface film.

Another mechanism involving film rupture has been proposed (61). Whereas the previous model was concerned only with crack tip processes, this mechanism also involves processes occuring ahead of the crack tip. This mechanism may be summarized as follows: (1) Film rupture occurs when an initial mechanical tensile stress is applied to an alloy in the passive state exposed to a corrosive medium. (2) Retarded repassivation of film rupture sites is caused by the repeated cyclic load. (3) Anodic dissolution then occurs at film rupture sites. This dissolution is accelerated by galvanic coupling to large passive areas. (4) Vacancies are formed at the rupture sites because of the anodic dissolution. (5) Divacancy formation occurs from a

supersaturation of surface vacancies due to migration of these surface vacancies to critical lattice sites. Diffusion and/or reversed slip processes due cyclic loading assist this migration. Cyclic loading can also form vacancies at internal sources. (6) Because of accumulation of divacancies on prismatic planes, brittle crack propagation by cleavage-like fracture under conditions of plane-strain then proceeds. A schematic diagram of this mechanism is given in Figure 2.9.

Mechanism of Surface Absorption of Aggressive Species

One final mechanism for environmentally assisted fatigue crack growth is that of surface energy reductions due to the adsorption of an aggressive chemical species. The adsorption of such a species (especially atomic hydrogen) serves to lower the local bond strength of a material and thereby increases the fatigue crack growth rate of that material. Hydrogen effects on crack growth have been observed mainly in steels, aluminum alloys and titanium alloys (62-71).

The effect of a water environment on the fatigue cracking of a cast steel has been associated with gases that were being evolved from the crack tip as a sample was being cyclically loaded (68). Some of the gas was collected and analyzed. It was found that hydrogen was being liberated from the crack tip. This finding was

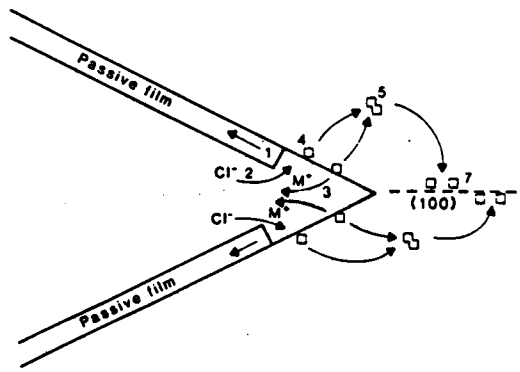

Figure 2.9 Schematic of Jones' mechanism for corrosion fatigue crack propagation.

interpreted as indicating a hydrogen embrittlement process in the cyclically loaded steel. Corrosion fatigue studies on two titanium alloys showed that as the load on a fatigue specimen was increased the measured potential of the sample became more cathodic (69). This again indicates the possibility of a hydrogen embrittlement mechanism for corrosion fatigue because as the load was increased, the surface area in the new crack tip region was enlarged which allowed more hydrogen to be adsorbed onto a specimen. In three separate studies by several investigators (70-72), it was found that as the applied cathodic current was increased on various structural and high strength steels fatigued in a corrosive environment, the fatigue crack growth rate of the steel specimens was increased.

Just as there are various ways that an environment can interact with a material to increase fatigue crack growth rates, there are various ways in which the environment degradation of a material and the cyclic loading of a material can interact in order to fail a component. The first of these interactions is called true corrosion fatigue. This term identifies behavior where fatigue crack growth rates are enhanced by the presence of an aggressive environment through a synergistic action of corrosion and cyclic loading (73).

True corrosion fatigue behavior is characterized by an environmental induced change on the values for C and n in the Paris equation. This effect is shown in Figure 2.10 (a). True corrosion fatigue behavior has been observed in alloy systems such as titanium (47-49) and aluminum (44-46, 74-76). True corrosion fatigue is observed when the applied stress in fatigue loading is below the K_{ISCC} (stress intensity need to induce SCC) for a given alloy.

The second type of environment-cyclic loading interaction is called stress-corrosion fatigue. Stress-corrosion fatigue describes static load stress corrosion under fatigue conditions. Crack extension by stress corrosion occurs whenever the stress intensity in the cycle is above K_{ISCC}. This type of fatigue behavior is characterized by a "bump" in ΔK vs. da/dN curve as shown in Figure 2.10 (b). Stress corrosion fatigue has been observed in steels (40-43) and titanium alloys (77). Clearly both true corrosion fatigue and stress-corrosion fatigue can exist in the same material. A typical ΔK vs. da/dN curve for such a process is shown in Figure 2.10 (c). Either true corrosion fatigue or stress-corrosion fatigue could be induced in a titanium alloy by changing the frequency and R-ratio (ratio of minimum to maximum load) of the fatigue loading (67). This has been also

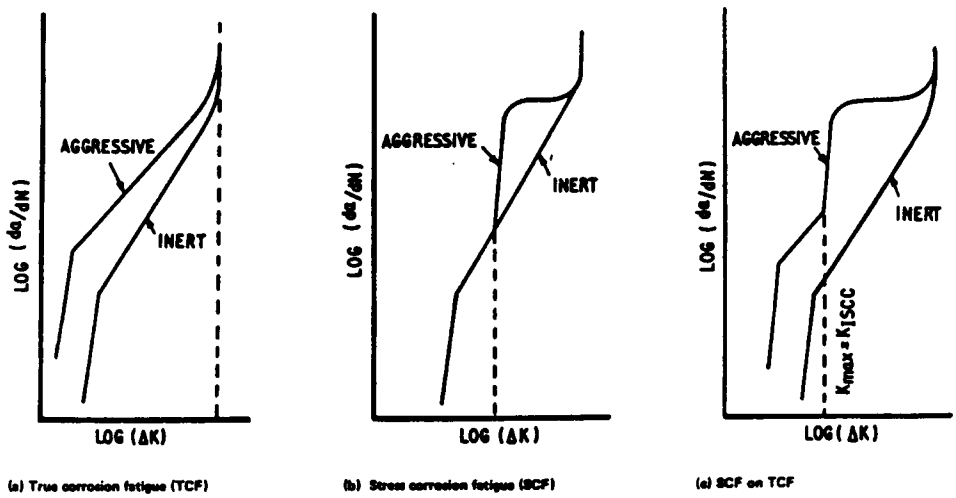

(a) True corrosion fatigue (TCF) (b) Stress corrosion fatigue (SCF) (c) SCF on TCF

Figure 2.10 Schematic illustrations of basic types of corrosion fatigue behavior.

observed in steels (73).

The role of the environment for a given material is the same (either hydrogen embrittlement or anodic dissolution) in both true corrosion fatigue (TCF) and stress-corrosion fatigue(SCF). Both TCF and SCF serve to expose fresh metal so that environment interactions may occur. In stress-corrosion fatigue, fresh metal is exposed in the crack tip stretch zone when K_{ISCC} is exceeded. True corrosion fatigue provides fresh metal surface through the formation of slip bands and striations due to cyclic loading.

Exposure to salt water environments generally increases the fatigue crack growth rate of metals and alloys. This has been observed in aluminum alloys (42, 78), steels (58, 70, 78, 79) and copper alloys (22-24). The application of an anodic potential also accelerates the fatigue crack growth of steels (58, 78, 80) due to the increased dissolution of material at the crack tip. The imposition of a cathodic potential onto a corrosion fatigue cell has varying effects according to the specific material. In some structural steels, cathodic protection served to slow the anodic dissolution rate and decelerate crack growth (80-84). However, in other steels (70, 71), the fatigue crack growth rate was increased as a cathodic current was applied. This

increase is though to be due to an increase in the amount of hydrogen adsorbed at the crack tip.

In summary, mechanisms of both fatigue crack initiation and propagation of ductile material seem to depend for the most part on localized slip at and around the crack tip. Exposure to aggressive environments accelerates the nucleation and propagation processes. The creation of fresh metal surfaces by slip allows this environmental interaction by either anodic dissolution or hydrogen embrittlement. The three major mechanisms for environmental interaction seem to correspond to three different regions of a polarization plot. Preferential dissolution of slip bands corresponds to the active region; film rupture, with the passive region and hydrogen embrittlement, with the immune region. This correlation suggests that when corrosion fatigue experiments are conducted, corresponding polarization studies should be done in order to determine what corrosion state a metal is in given an environment of a particular pH and potential. This can then give an indication as to what mechanism of environmentally assisted fatigue crack propagation is occurring.

The way the fatigue cycles and the environment interact in the growth of a crack depends on the applied stress intensity. If the applied stress intensity is

below K_{ISCC}, then a synergistic reaction occurs between cyclic loading and the environment which results in true corrosion fatigue. If the loading is above K_{ISCC}, then a combination of stress corrosion cracking and mechanical fatigue occurs which is termed stress corrosion fatigue.

MATERIALS AND METHODS

The effects of applied potential and pH on the failure of a copper-nickel alloy, CA 706, in an aqueous solution containing 3.5% NaCl were investigated. Samples were tested under conditions of cyclic and monotonic loading. In addition, polarization studies in 3.5% NaCl aqueous solutions of varying pH's were conducted on the same alloy. The composition and mechanical properties of the CA 706, also referred to as 90-10 copper-nickel, used in this study are given in Table 3.1. The typical microstructure of the test material is shown in Figure 3.1. The material was received in the hot rolled and annealled condition.

Cyclic Loading Experimentation

Compact-tension specimens of 90-10 copper-nickel were machined from a plate of 0.090" thickness to the dimensions shown in Figure 3.2. The thickness of the specimens was determined by their proposed industrial application rather than by ASTM requirements. The application is for the copper-nickel alloy to be used as thin sheets of 90-10 copper-nickel welded to steel ship hulls. These sheets will serve as a cladding material and protect the steel from corrosion.

TABLE 3.1 Composition and Mechanical Properties of 90-10 Copper Nickel

Cu	87.77%
Ni	10.60%
Fe	1.14%
Mn	0.294%
Zn	0.056%
C	0.056%
Co	0.026%
Si	0.019%
Sn	0.009%
Pb	0.006%
P	0.003%
S	0.002%
Al	0.002%
Mg	0.001%

Yield Strength	30.2 ksi
Ultimate Tensile Strength	51.8 ksi
% Elong in 2 in.	32.0
Hardness	R 51

Figure 3.1 Typical microstructure of 90-10 copper-nickel used in experiments.

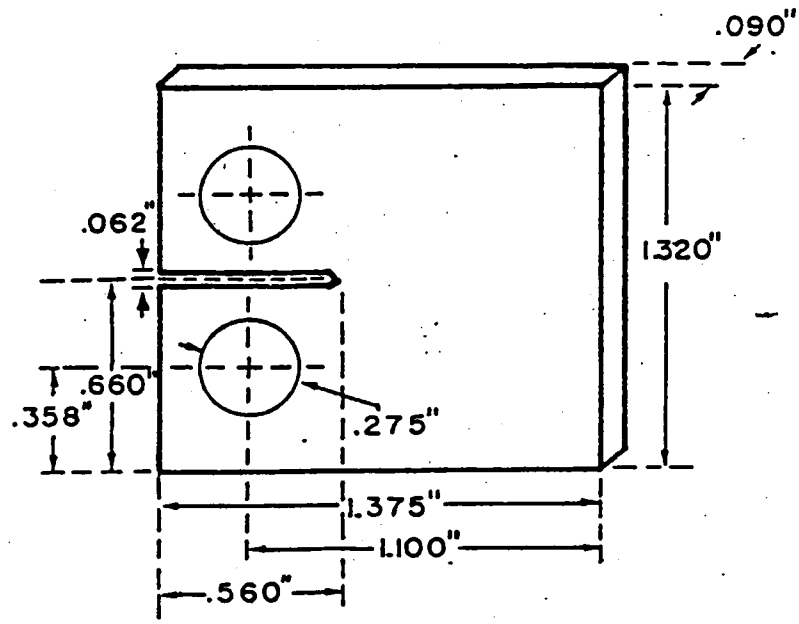

Figure 3.2 Geometry of compact tension specimens.

Mode I tension-tension fatigue tests were conducted on samples exposed to a 3.5% sodium chloride aqueous solution. Test procedures used a MTS servohydraulic machine operating under load control to apply the desired stress cycles. The aqueous environment was prepared by combining 35 grams of NaCl with 965 ml of distilled water. The environment was maintained around the fatigue specimen by using a plexiglas test chamber which enclosed the specimen and contained the sodium chloride solution (Figure 3.3). During testing, the solution was regularly flushed and replenished.

Prior to each fatigue test, the surface of the compact tension specimen to be tested was ground and polished to a 1.0 micron finish. The specimens were tested at a frequency of 15 Hz and loads were applied in a sinusoidal wave form. All samples were tested with a R-ratio (maximum load/minimum load) of 0.4. The anodically polarized samples were cycled between stress intensities of 15.88 MPa$\sqrt{m}$ and 6.36 MPa$\sqrt{m}$(Pmax = 1110 N and Pmin = 444N). The cathodically polarized samples were cycled between stress intensities of 12.70 MPa$\sqrt{m}$ and 5.09 MPa$\sqrt{m}$ (Pmax = 888 N and Pmin = 355.2 N). The compact tension samples were polarized using a Model 173 E.G.&G. Potentiostat/Galvanostat to apply and control the current to the sample. Wires led from the potentiostat

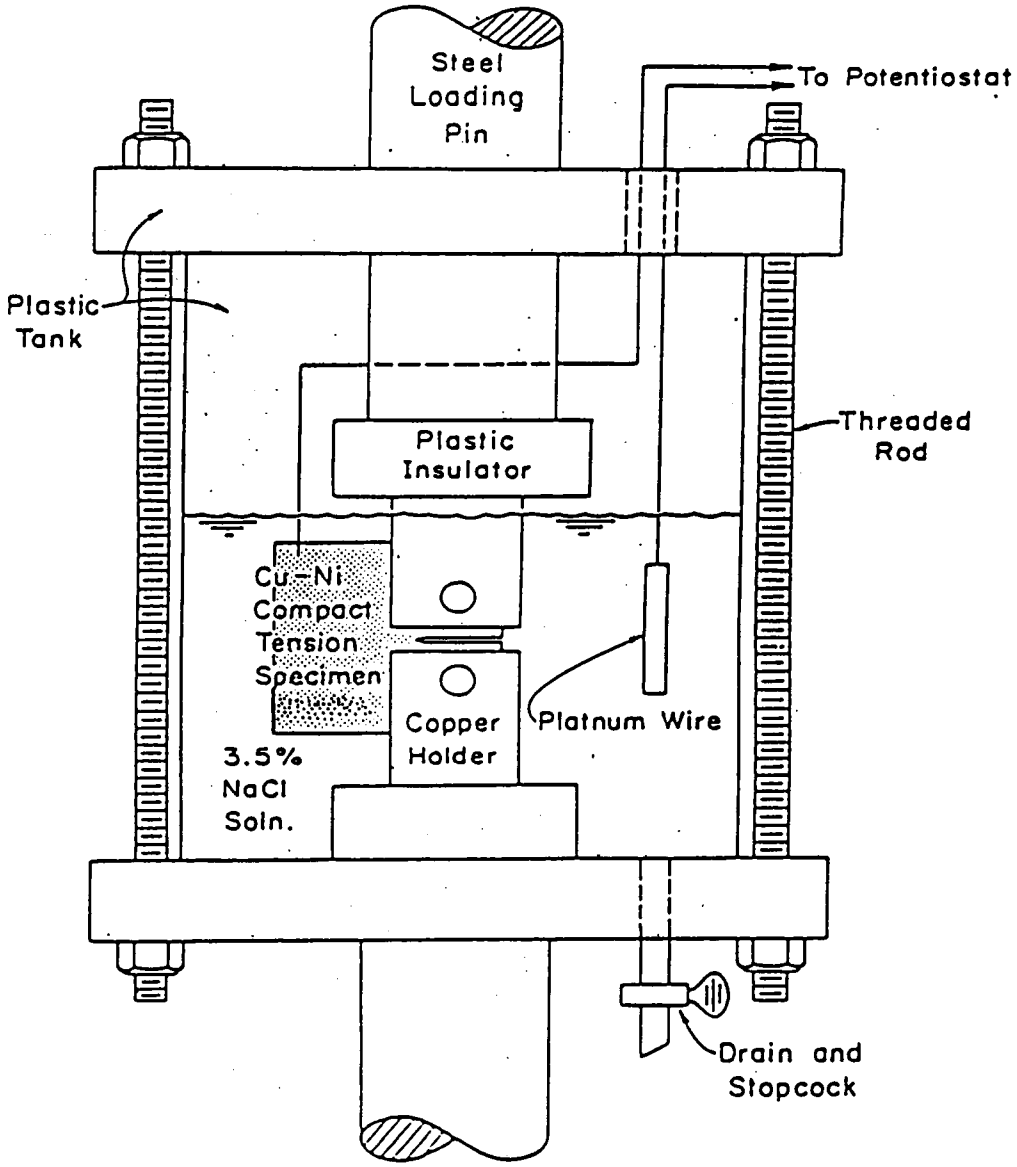

Figure 3.3 Schematic of plexiglass test chamber.

into the test chamber where they were connected to the compact-tension specimen and an inert platinum electrode. The anodically polarized samples were tested at current densities of 0 $\mu A/cm^2$, 181 $\mu A/cm^2$, 331 $\mu A/cm^2$, 956 $\mu A/cm^2$ and 1810 $\mu A/cm^2$. The cathodically polarized samples were tested at current densities of 0 $\mu A/cm^2$, 331 $\mu A/cm^2$ and 956 $\mu A/cm^2$. At least two tests were made at each current density to ensure the reproducibility of results. The corrosion products which accumulated during testing were collected after the tests were complete. The collected products were subjected to ESCA analysis. The fracture surfaces of the failed fatigue specimens were examined with a JEOL-35C scanning electron microscope.

Monotonic Loading Experimentation

Constant extension rate (CERT) tests were conducted on compact tension samples of 90-10 copper nickel of the same dimensions as shown in Figure 3.2. These tests were conducted on an Instron screw driven tensile testing machine. An extension rate of 0.0005 cm/min was used. The plexiglas test chamber (Figure 3.3) was used to maintain the aqueous environment and again, each specimen was ground and polished to a 1.0 micron surface finish prior to testing. The tests were carried out in neutral 3.5% sodium chloride solution (pH = 6.6) and in 3.5% sodium chloride solution titrated with hydrochloric acid

to a pH of 1.0. The titration was carried out while a magnetic stirrer agitated the solution as the hydrochloric acid was added. The pH of the solution was monitored with a Fisher Acumet Model 610A pH meter. The samples were both anodically and cathodically polarized to current densities of 1810 $\mu A/cm^2$ and 200 $\mu A/cm^2$ respectively using a E.G.&G. Model 173 Potentiostat/ Galvanostat. The environmental test matrix for monotonic loading is given in Table 3.2. The experimental set up for monotonic loading is shown in Figure 3.4. The fracture surfaces of the failed specimens were examined with a JEOL-35C scanning electron microscope.

Polarization Studies

The first set of polarization studies was performed on a sample of 90-10 copper-nickel with a Monel weld. This weld was produced by attaching two copper nickel sheets to a steel plate which was subsequently removed (see Figure 3.5). Anodic polarization studies were performed to compare the corrosion characteristics of the heat affected zone to those of the base metal on the weld joint. This was done in order to evaluate the effect of welding on the corrosion of the 90-10 copper-nickel sheeting. The surface of the sample was polished to a 1.0 micron finish prior to testing. The polarization studies were performed with an E.G.&G. Model 173

TABLE 3.2 Test Matrix for Monotonic Loading.

	pH 1.0	pH 6.67
200 $\mu A/cm^2$, cathodic	2 tests	2 tests
0 $\mu A/cm^2$	2 tests	2 tests
1810 $\mu A/cm^2$, anodic	2 tests	2 tests

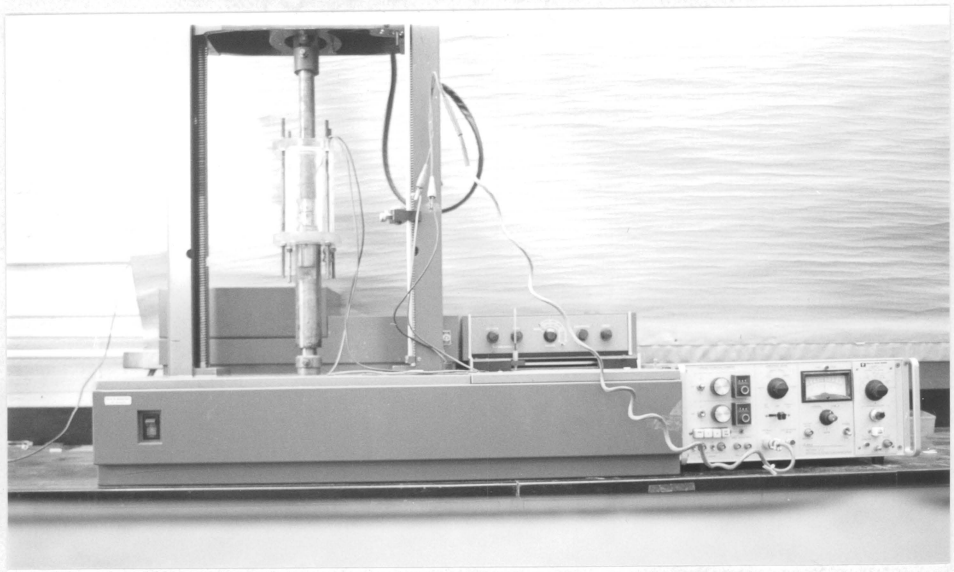

Figure 3.4 Experimental set-up for monotonic loading.

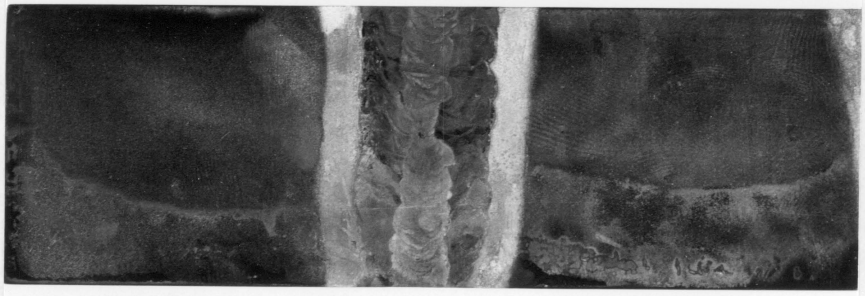

Figure 3.5 Copper-nickel sample with monel weld used in Potentiostatic studies.

Potentiostat/Galvanostat at a scan rate of 5 mv/10 min. A standard saturated calomel electrode was used as the reference electrode and a platinum wire was used as the counter electrode. The tests were carried out in a 3.5% sodium chloride solution. A schematic of the experimental set up for these studies is shown in Figure 3.6.

A second set of potentiostatic studies were performed to determine the effect of pH on the anodic polarization of 90-10 copper-nickel. A compact tension specimen was used in these studies (Figure 3.2). The surface of the sample was ground and polished to a 1.0 micron finish prior to testing. The polarization studies were performed using an E.G.&G. Model 173 Potentiostat with a scan rate of 10 mv/10 min. The experiments were carried out in solutions of 3.5% sodium chloride with the pH of 6.6, and in 3.5% sodium chloride titrated with hydrochloric acid to a pH of 3.0 and to a pH of 1.0. The experimental set-up is similar to that shown in Figure 3.6 except for differences in the specimen used and pH variations of the solution.

A third set of polarization studies investigated the effect of pH on the repassivation of 90-10 copper-nickel. A compact tension specimen was again used for this study. The sample, which was polished to a 1.0 micron surface

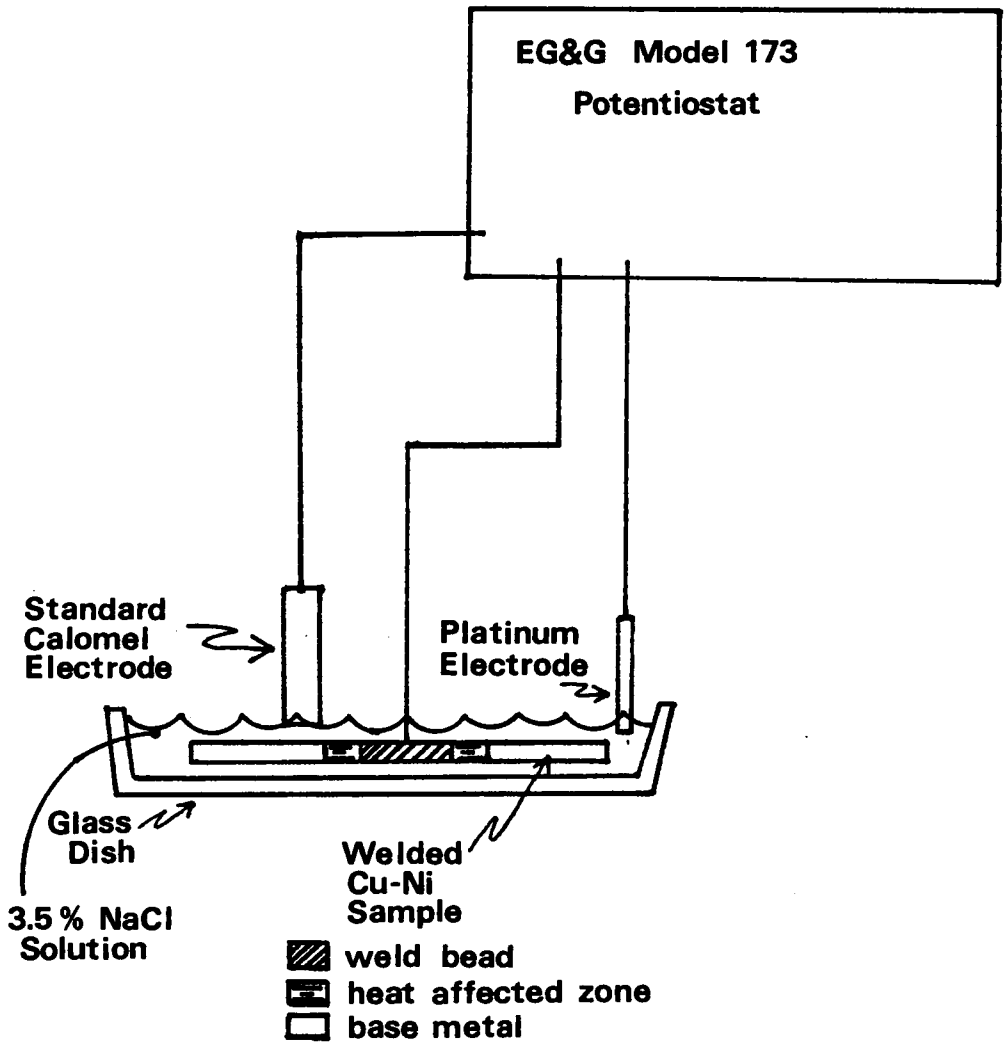

Figure 3.6 Schematic of experimental set-up for Potentiostatic studies of copper-nickel with monel weld.

finish, was placed in solutions of 3.5% sodium chloride with a pH of 6.6 and in 3.5% sodium chloride solutions titrated with hydrochloric acid to pH's of 1.0, 2.0, 3.0 and 4.0. The 3.5% sodium chloride solutions were also titrated with sodium hydroxide to pH's of 9.0 and 11.0 so that basic pH's could be examined. As the applied current was increased in steps of $10^{X+0.2}$ μA/5 min; where x = 0, 0.2, 0.4, ...; the pH of the bulk solution was monitored and the formation of surface films was observed. The pH was monitored with a Fisher Acumet Model 610A pH meter and the current was applied with an E.G.&G. Model 173 Potentiostat/Galvanostat. The experimental set up for these studies is shown in Figure 3.7.

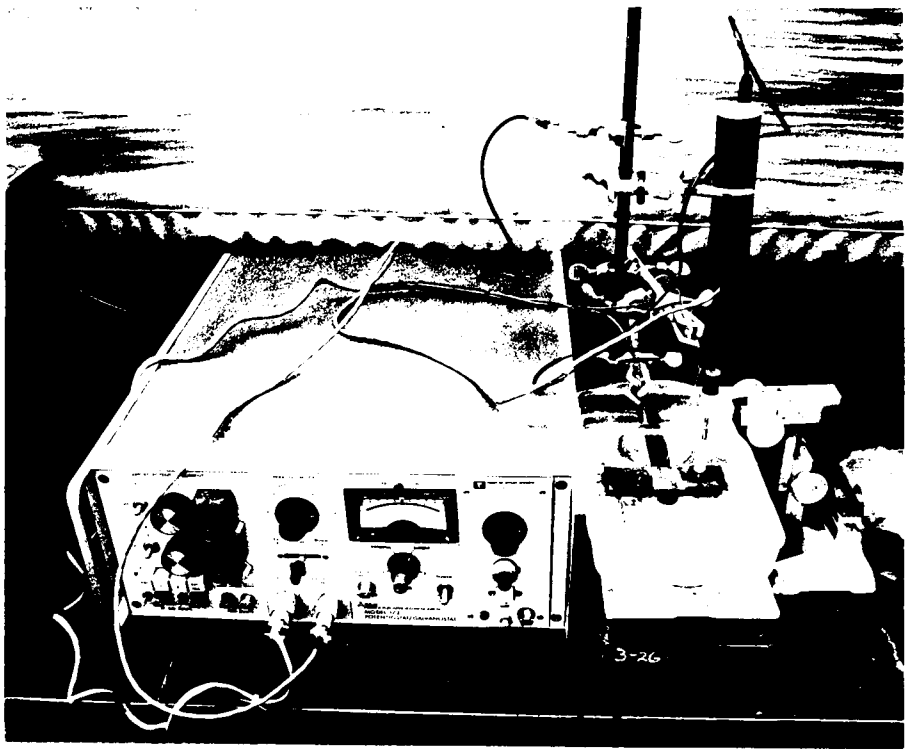

Figure 3.7 Experimental set-up of polarization and pH studies on copper-nickel specimen.

EXPERIMENTAL RESULTS

Fatigue Tests with Anodic Polarization

The results of the fatigue tests made with applied anodic currents show that the corrosion fatigue life of 90-10 copper-nickel decreases as the applied anodic current is increased. The data from these tests is presented in Figure 4.1 as the number of cycles to failure as a function of applied current. It was found that the maximum applied anodic current reduced the fatigue life by almost 70% compared to the lifetime obtained on samples tested with no applied current. A change in the slope of the life vs. applied current curve was also observed. The slope of the curve at current values less than 200 $\mu A/cm^2$ is much greater than the slope for currents greater than 500 $\mu A/cm^2$.

Fractographic analysis of the failed specimens revealed that the fracture mode underwent a transition as the applied anodic current was increased. Figures 4.2 and 4.3 show the fatigue crack initiation regions of 90-10 copper nickel compact tension specimens subjected to 0 $\mu A/cm^2$ and 1810 $\mu A/cm^2$ of anodic current respectively. The fatigue cracks initiated in a predominantly transgranular mode when no current was applied, but as the anodic current was increased, the

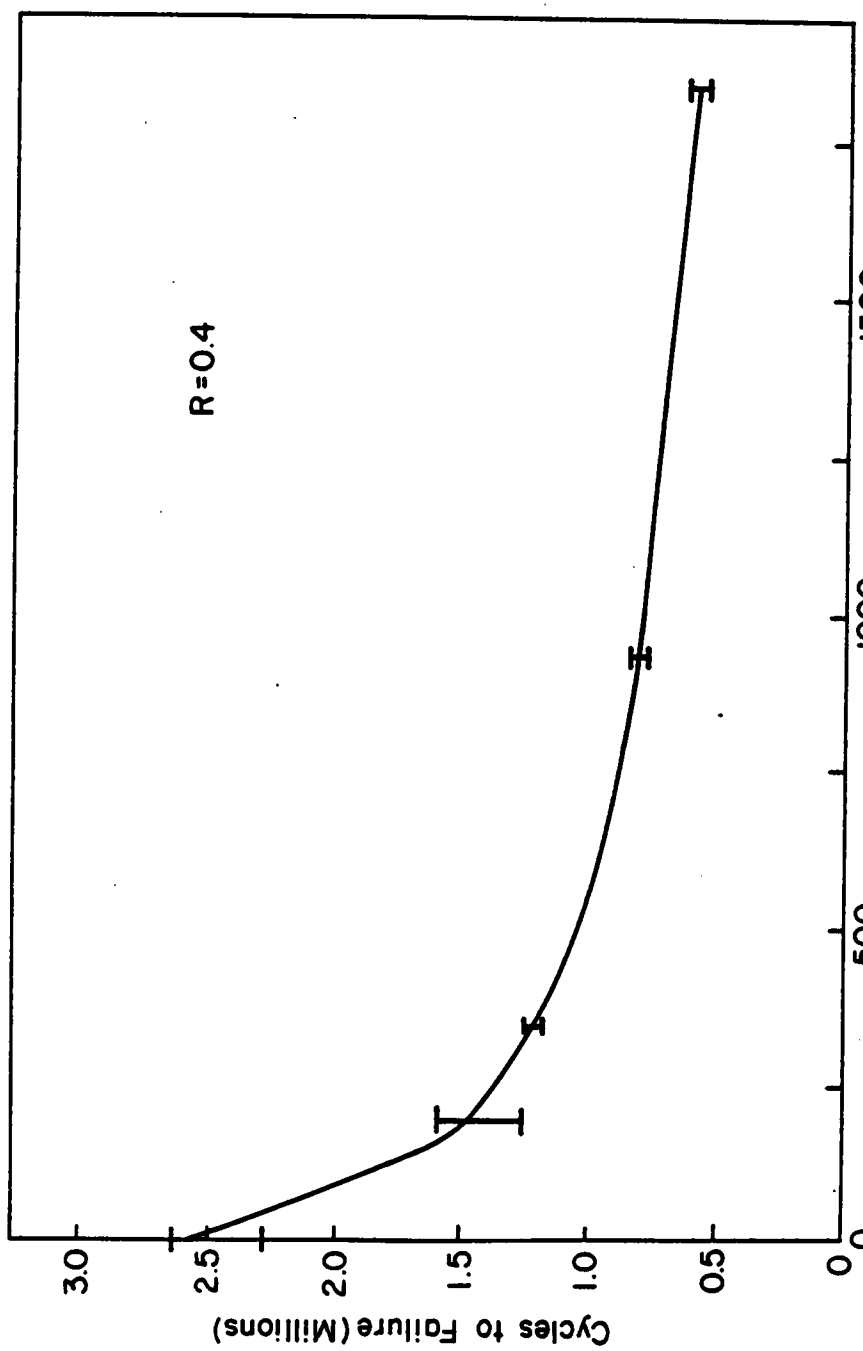

Figure 4.1 Corrosion fatigue life of 90-10 copper nickel as a function of applied anodic current.

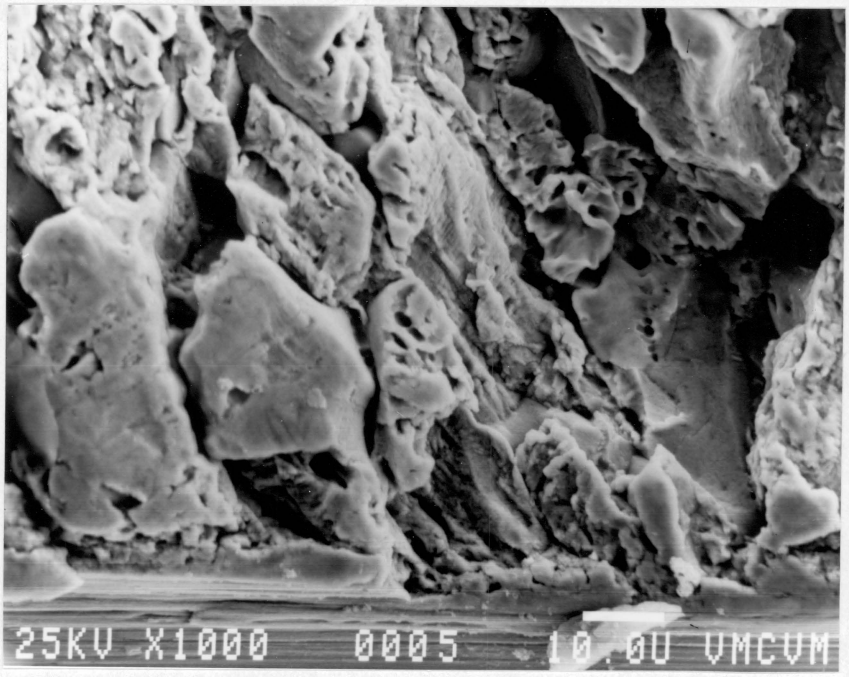

Figure 4.2 Transgranular initiation at 0 $\mu A/cm^2$

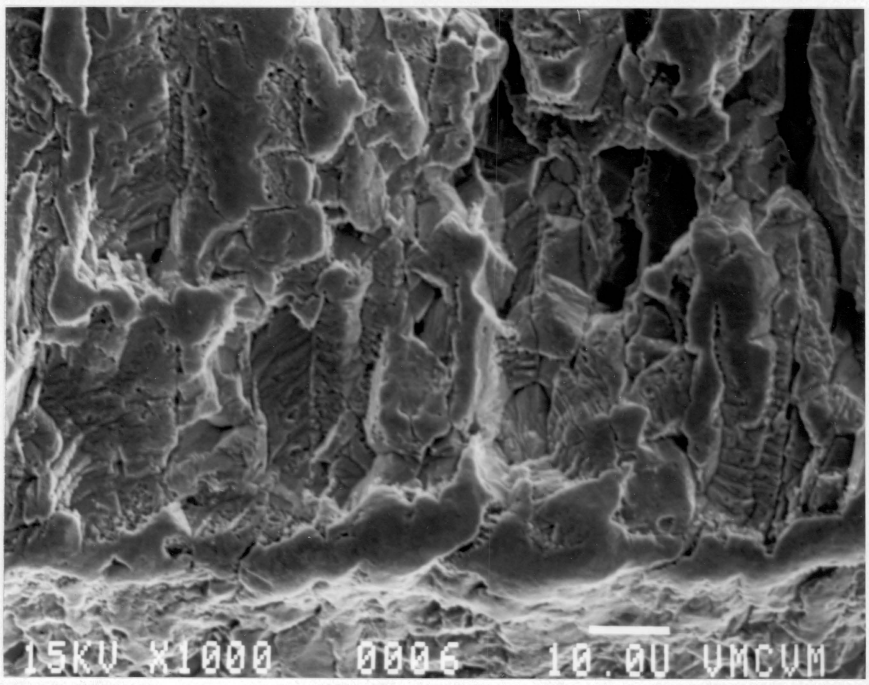

Figure 4.3 Mixed (transgranular and intergranular) initiation at 1810 $\mu A/cm^2$, anodic.

cracks initiated in a mixed (transgranular and intergranular) mode. A transition in fracture mode was also observed in the fatigue crack propogation regions of these samples. Figure 4.4 shows a predominantly transgranular fracture mode in samples tested at 0 $\mu A/cm^2$ of applied while Figure 4.5 shows a predominantly intergranular fracture mode in specimens tested at 1810 $\mu A/cm^2$ of applied anodic current. A continuous increase in the amount of intergranular fracture was observed as the applied anodic current was increased (Figure 4.6). When no current was applied ten percent of the sample failed by intergranular fracture. As the anodic current was increased to 1810 $\mu A/cm^2$, the amount of intergranular fracture increased to ninety-five percent. Figure 4.6 also reveals a change in the rate of change of the percentage of intergranular fracture with an increase in applied current. The slope of the percentage of intergranular fracture vs. applied current curve is steeper at currents less than 500 $\mu A/cm^2$ than the slope at currents greater than about 750 $\mu A/cm^2$.

Further fractographic studies revealed the presence of second-phase particles in the intergranular fracture regions of the failed fatigue specimens (Figures 4.7 a and b). These particles were believed to be an iron rich phase based on the results of previous studies. This

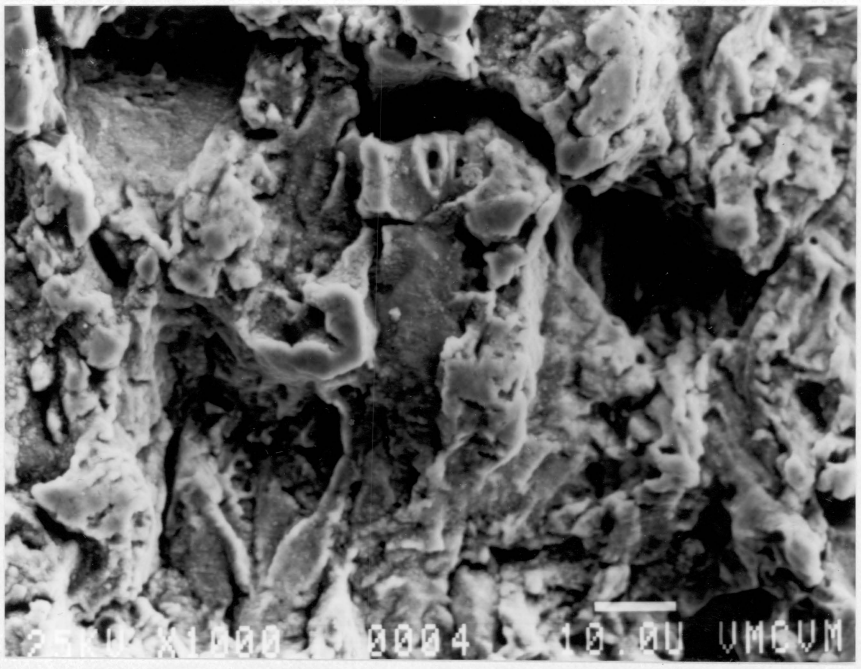

Figure 4.4 Stage II Fatigue crack propagation for sample tested at 0 $\mu A/cm^2$. (10% intergranular fracture).

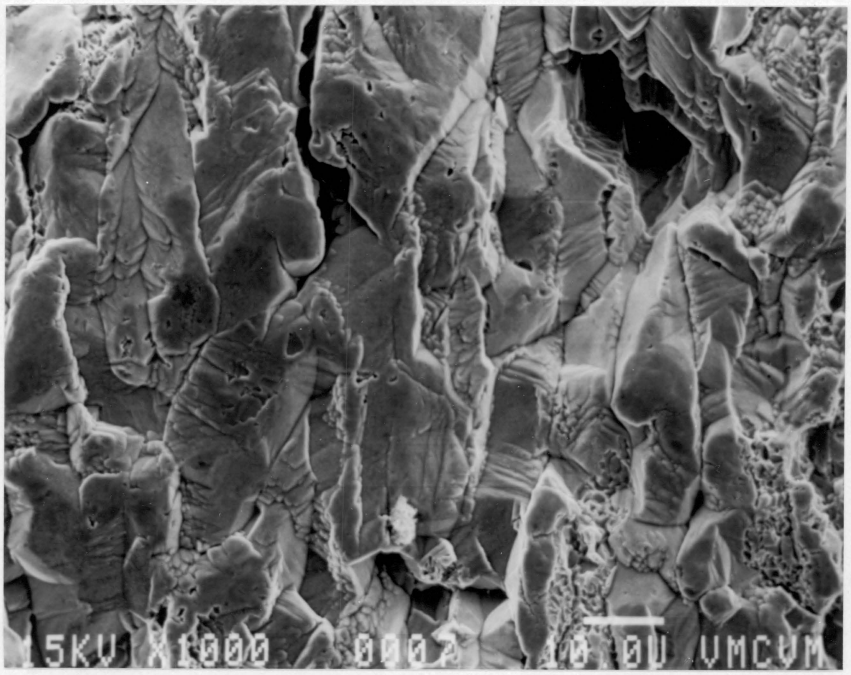

Figure 4.5 Stage II Fatigue crack propagation for sample tested at 1810 $\mu A/cm^2$, anodic. (95% intergranular fracture).

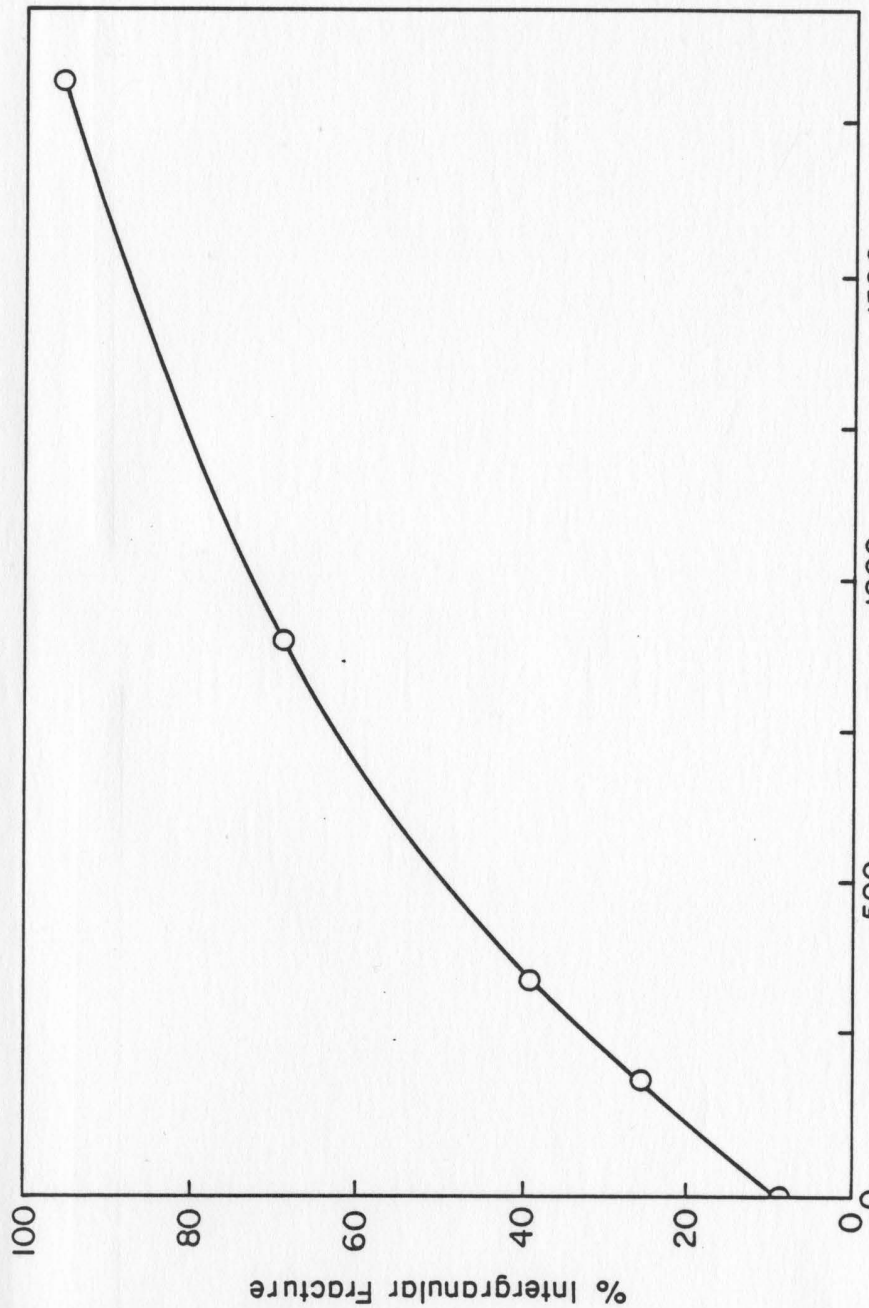

Figure 4.6 Percentage of intergranular fracture as a function of applied anodic current.

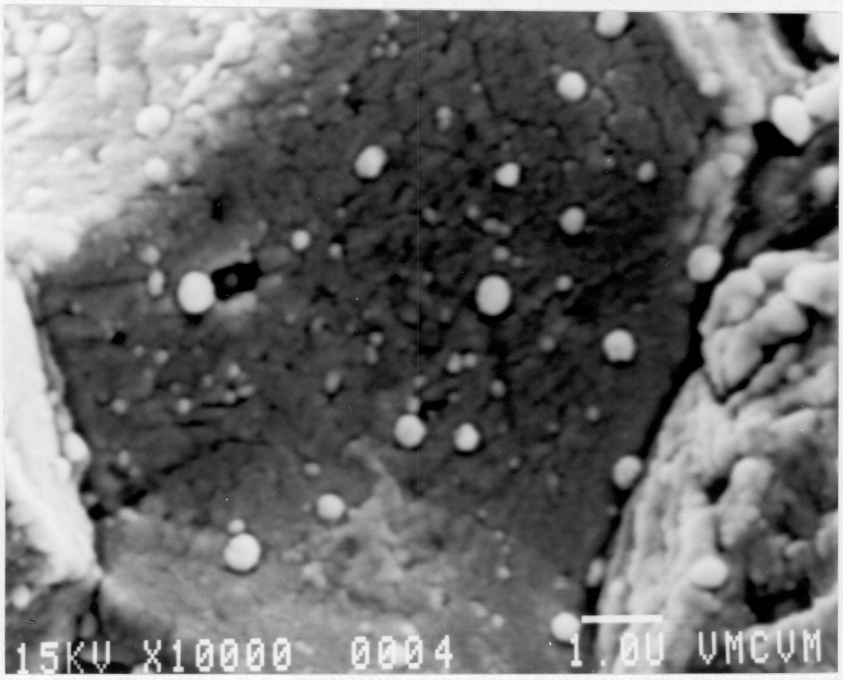

(a)

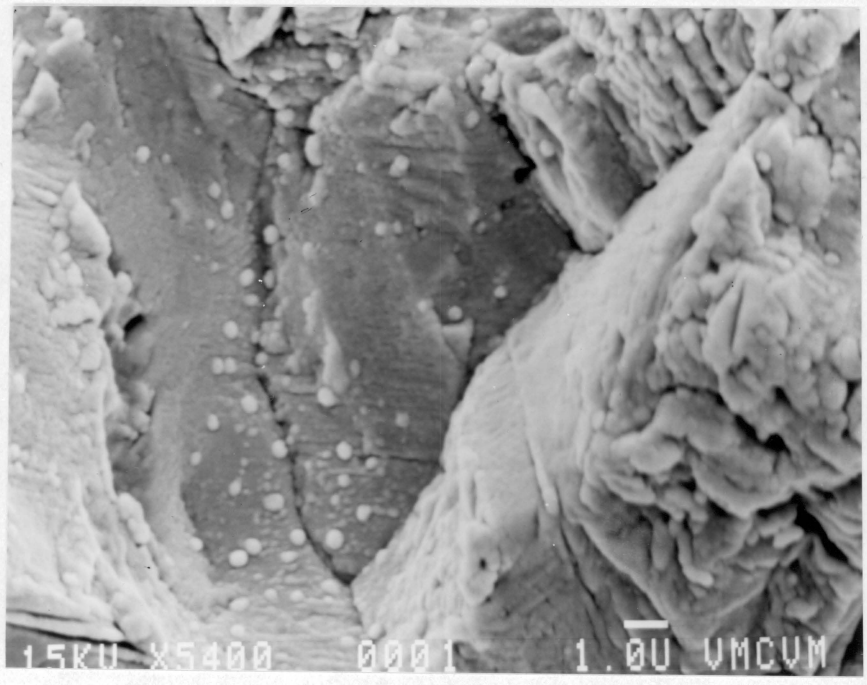

(b)

Figures 4.7 a & b Iron rich second phase particles on fracture surface of sample tested at 181 $\mu A/cm^2$ anodic.

hypothesis was confirmed by EDAX scans of an intragranular region and a grain boundary in a sample of the 90-10 copper nickel test material. Figure 4.8 is the scan made of the intragranular region and shows that the nickel content is greater than the iron content. Figure 4.9 is the EDAX scan of a grain boundary and reveals that the iron content is greater than the nickel content. Therefore, the second phase particles, which were observed mainly at grain boundaries, are probably iron rich. These particles were observed in abundance on the fracture surfaces of specimens subjected to levels of anodic current up to 331 $\mu A/cm^2$. However, as the anodic current applied to the specimens was increased, the number of particles observed decreased until finally at the maximum anodic current, very few particles remained on the fracture surfaces.

As the level of applied anodic current was increased, a number of trends in the nature of the corrosion products generated were observed through visual and ESCA analyses. The data from the ESCA scans of the corrosion products as well as brief description of the appearance of the corrosion products is shown in Table 4.1. At zero applied current the corrosion product was bright yellow. As the applied anodic current was increased, the corrosion product became progressively

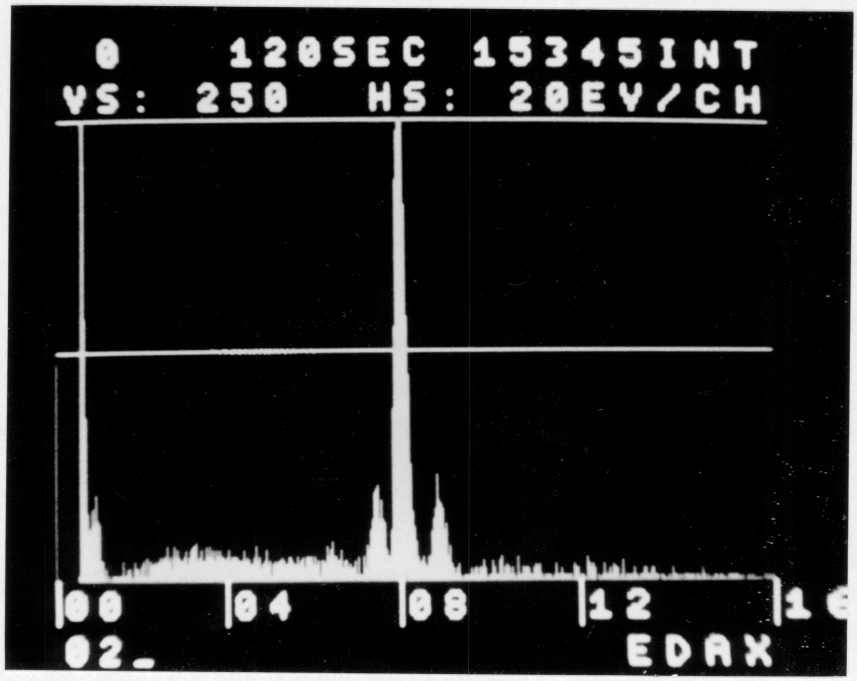

Figure 4.8 EDAX analysis of general surface of 90-10 copper nickel.

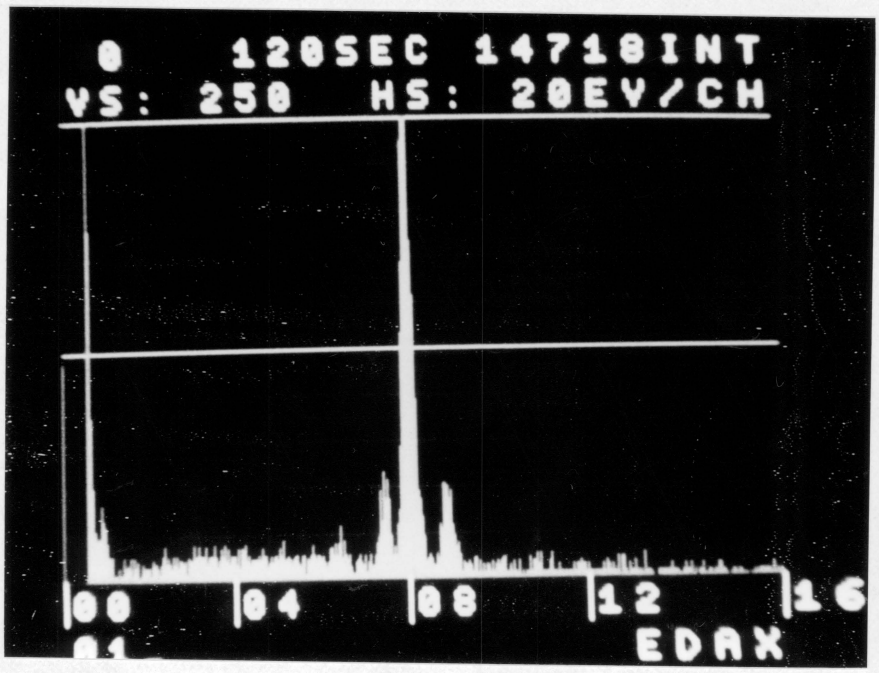

Figure 4.9 EDAX analysis of grain boundary in 90-10 copper nickel specimen.

TABLE 4.1 Data from ESCA scans of corrosion product.

CURRENT ($\mu A/cm^2$)	COLOR OF CORROSION PRODUCT	C 1s		Cl 2p		Cu 2p		Fe 2p		Ni 2p		O 1s	
		B.E.	%	B.E.	%	B.E.	%	B.E.	%	B.E.	%	B.E.	%
0	Yellow	285.0	49.8	199.3	2.8	944.8	1.2	711.6	4.6			531.5	41.6
181	Orange	285.0	29.7	198.9	1.9	934.1	0.9	711.8	12.0			530.2	55.5
331	Tan	285.0	49.7			933.7	1.7	711.3	6.2			530.5	42.4
956	Medium Brown	285.0	50.4					711.2	8.0			530.6	41.6
1810	Dark Brown	285.0	36.1			933.7	7.0	711.8	1.7	856.4	2.2	531.2	53.0
18100	Black	285.0	38.0			933.3	6.0			856.2	2.7	531.2	53.5

darker until it appeared black at the maximum applied current. This change in the color of the corrosion products corresponds to changes in the relative amounts of iron and copper in the corrosion products. The ratio of the relative amounts of these two species was obtained from ESCA data and was plotted as a function of applied anodic current in Figure 4.10. At zero applied current, the iron to copper ratio was approximately equal to four. As the applied anodic current was increased to 181 $\mu A/cm^2$ the iron to copper ratio increased drastically to a value more than thirteen. As the current was increased from this point, the iron to copper ratio decreased and at the highest anodic currents, asymptatically approached zero. At low current levels, chloride ions were also detected. As the current was increased, the amount of chloride decreased and at 331 $\mu A/cm^2$ of anodic current, chloride was no longer detectable. Nickel corrosion products were detected only at the very highest current levels.

Further metallographic observations were made on the surfaces and near surface regions of the failed compact tension specimens. At the lower applied anodic currents, slip band formation was observed on the surfaces perpendicular to the fracture surface as shown in Figures 4.11 and 4.12. Similar observations were not made at higher currents because the surface features were

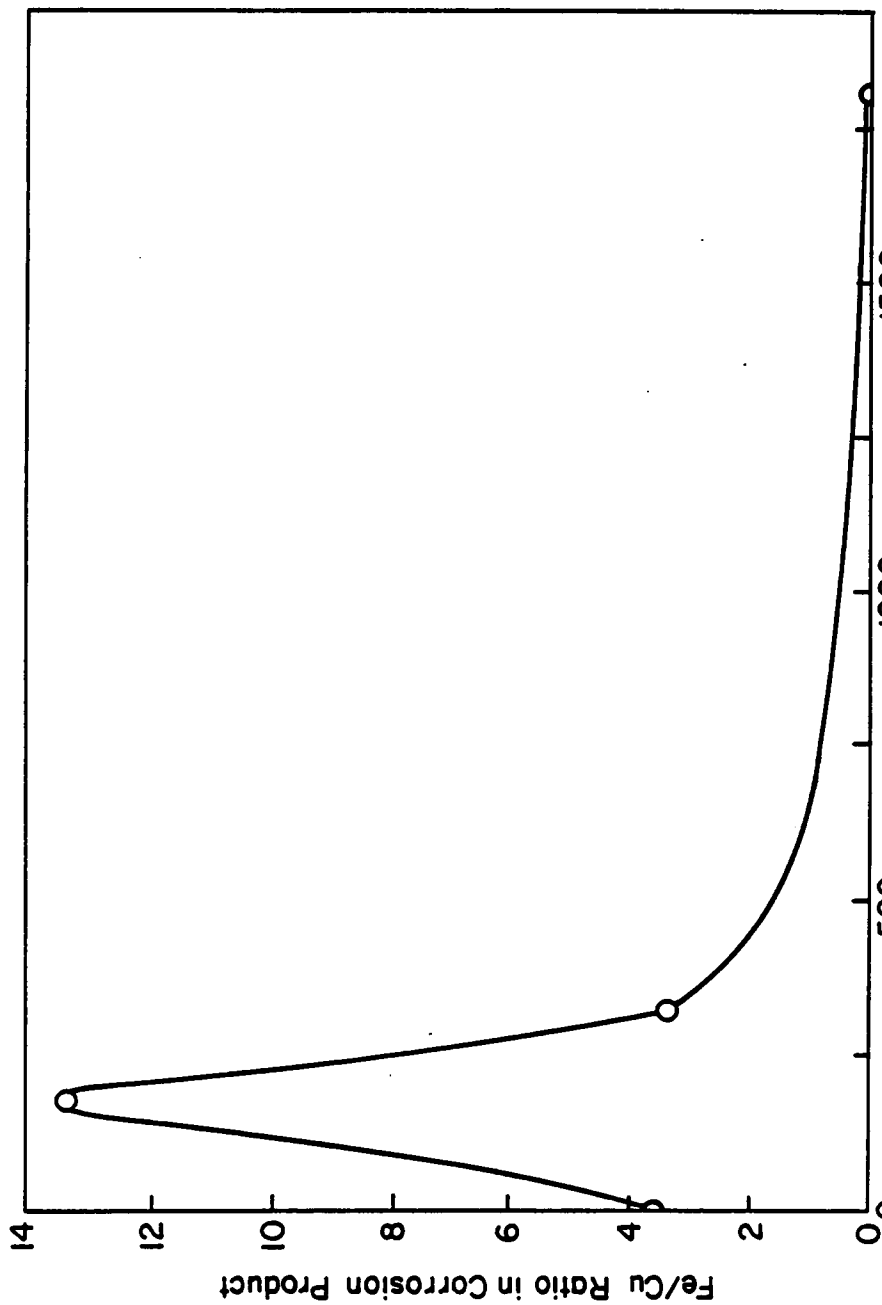

Figure 4.10 Iron to copper ratio in corrosion product as a function of applied current.

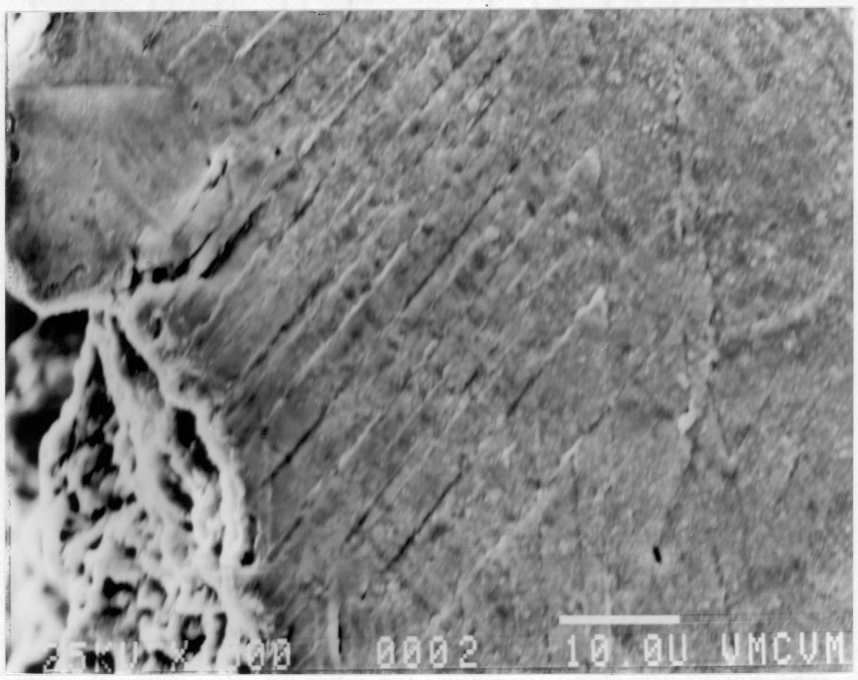

Figure 4.11 Slip bands observed on sample tested at 0 $\mu A/cm^2$.

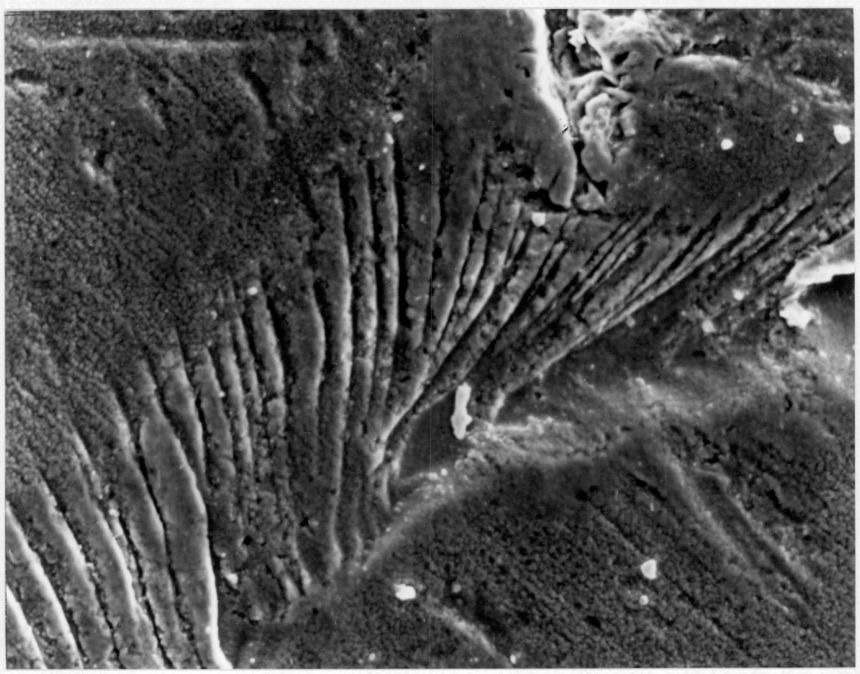

Figure 4.12 Slip bands observed on Cu-Ni specimen fatigued at 181 $\mu A/cm^2$, anodic.

obliterated by general corrosion of the sample. In all of the 90-10 copper nickel specimens fatigued under conditions of anodic polarization, the overload region was characterized by a ductile rupture failure mechanism as shown in Figures 4.13 and 4.14.

Fatigue Tests with Cathodic Polarization

The corrosion fatigue life of 90-10 copper nickel increased as the applied cathodic current was increased. The results from these tests are presented in Figure 4.15 as cycles to failure as a function of applied cathodic current. It was found that the maximum applied cathodic current of 956 $\mu A/cm^2$ increased the fatigue life of 90-10 copper nickel by about 23% over the life obtained in the zero applied current tests. The slope of the fatigue life vs. applied current curve was relatively constant over the region of testing.

Fractographic analysis of the specimens fatigued with an applied cathodic current showed that as the applied current was increased, the fracture mode underwent a transition. Figures 4.16 and 4.17 show the fatigue crack initiation regions for 90-10 Cu-Ni compact tension specimens tested at currents of 331 $\mu A/cm^2$ and 956 $\mu A/cm^2$, respectively. At 331 $\mu A/cm^2$ of applied cathodic current, the initiation fracture mode was a mixture of transgranular and intergranular while at

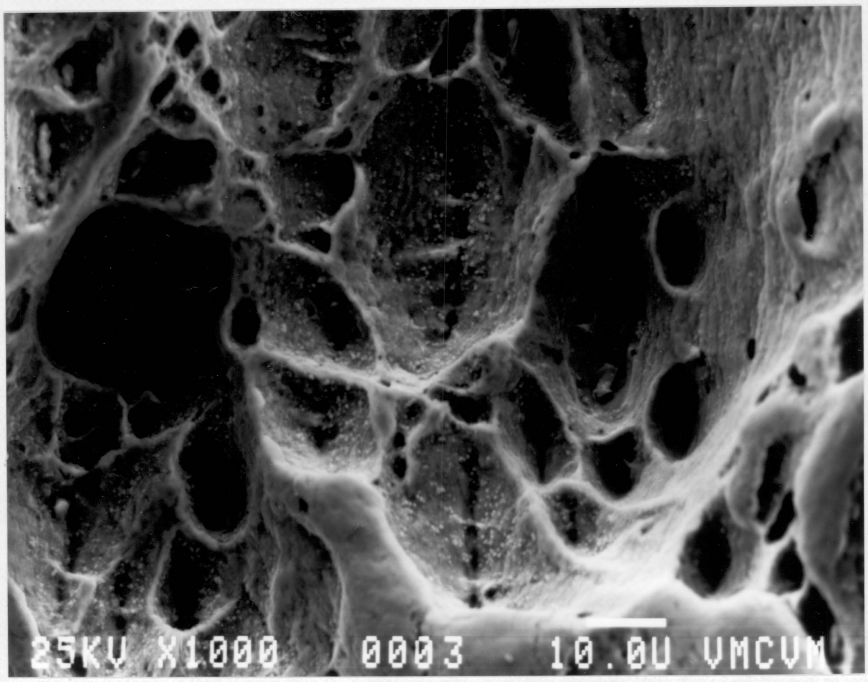

Figure 4.13 Typical overload regions at 0 $\mu A/cm^2$, anodic.

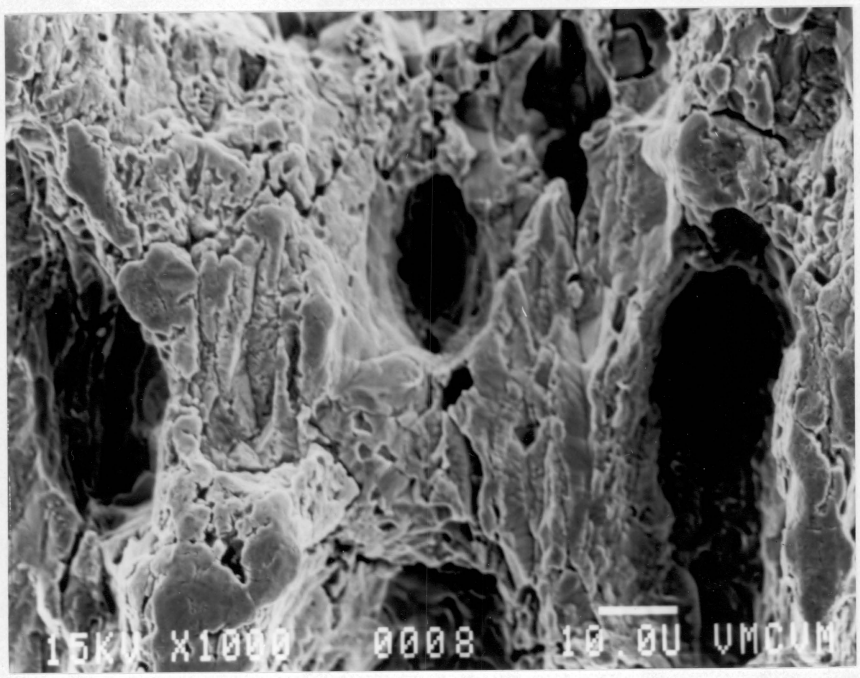

Figure 4.14 Typical overload regions at 1810 $\mu A/cm^2$, anodic.

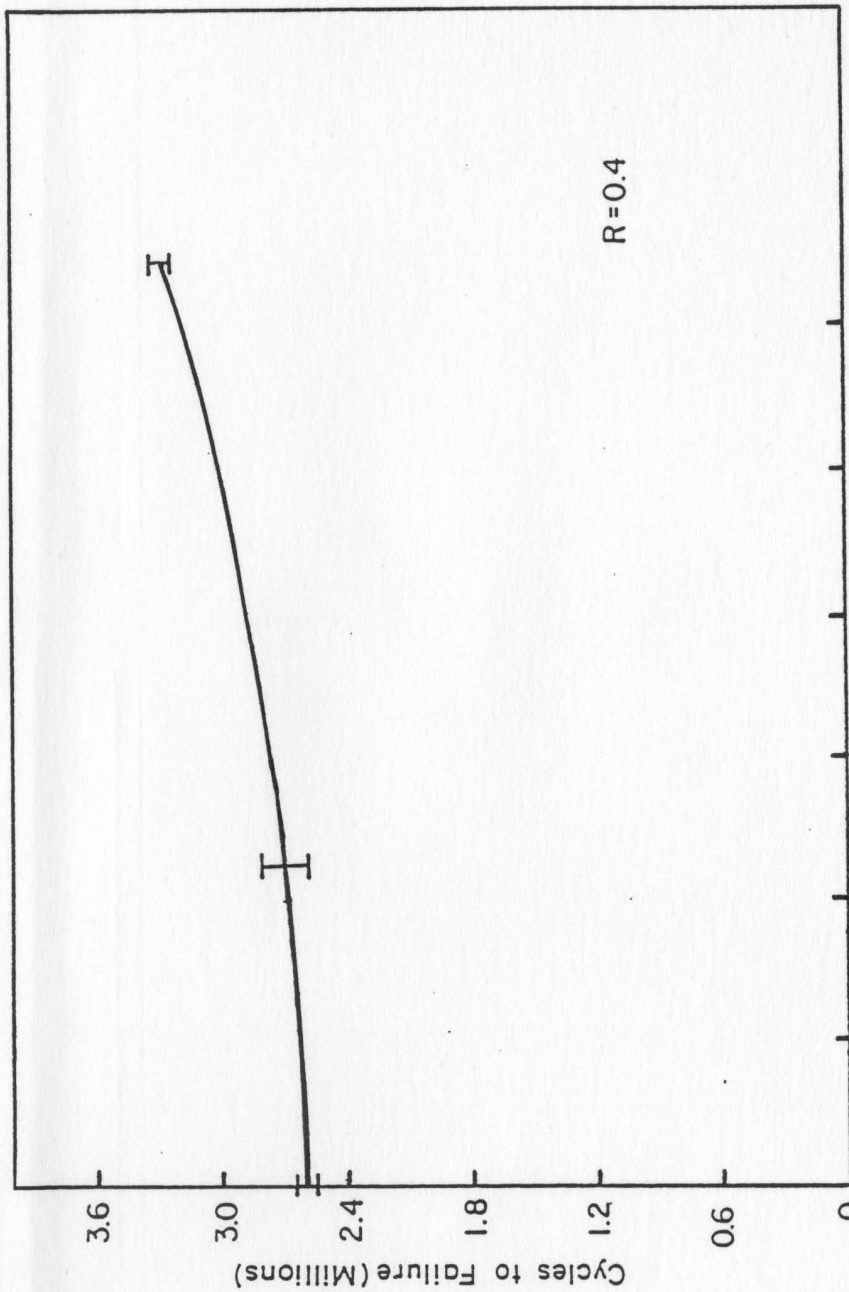

Figure 4.15 Corrosion fatigue life of 90-10 copper nickel as a function of applied cathodic current.

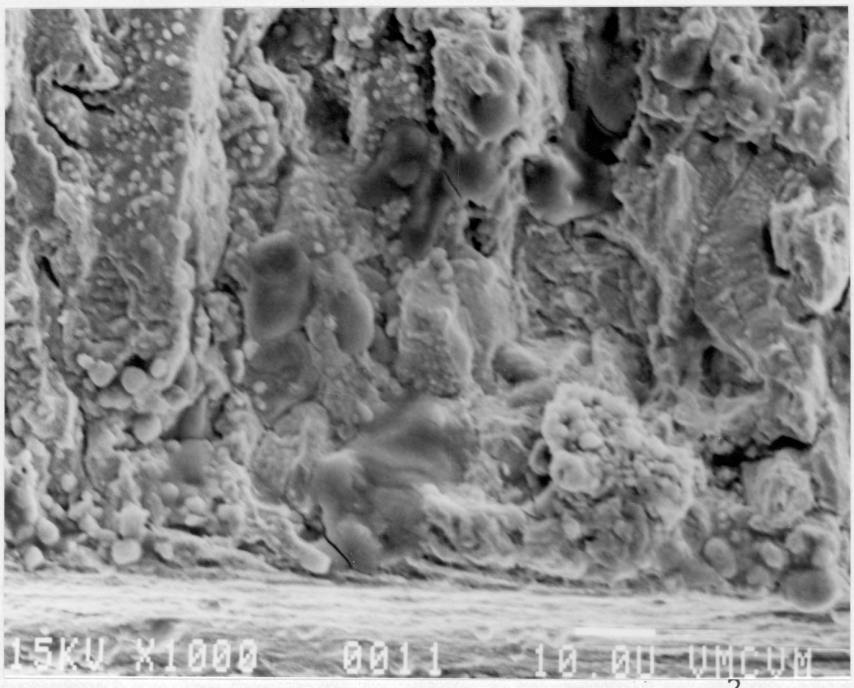

Figure 4.16 Mixed initiation at 331 μA/cm^2, cathodic

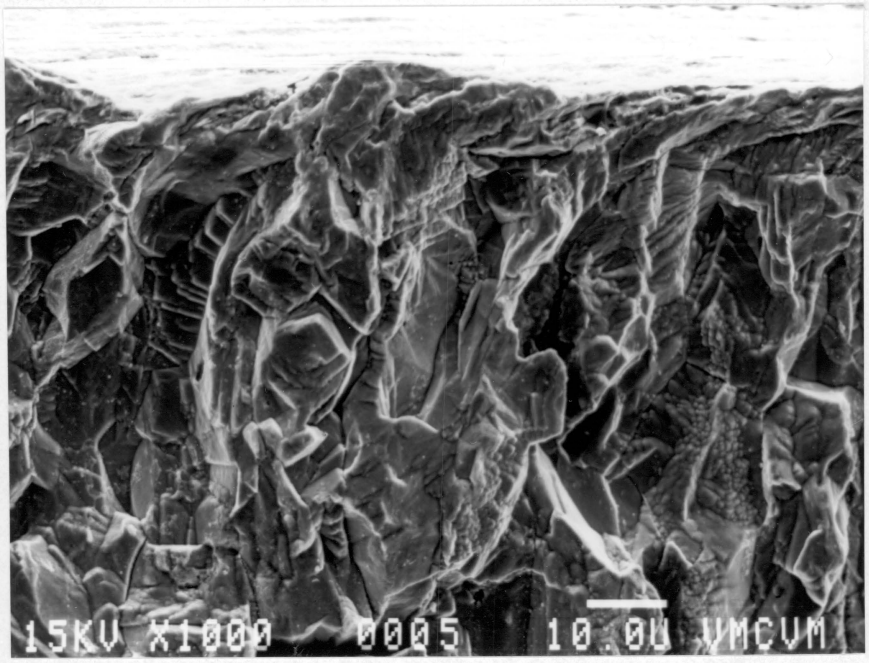

Figure 4.17 Intergranular initiation at 956 μA/cm^2, cathodic.

956 $\mu A/cm^2$, the initiation mode was almost totally intergranular. The fracture mode for fatigue crack propagation also changed with changes in applied cathodic current. Figure 4.18 shows the propagation region for a sample tested at 331 $\mu A/cm^2$ of cathodic current. The fracture mode at this current level was mixed intergranular and transgranular with approximately 35% intergranular. When the cathodic current was increased to 956 $\mu A/cm^2$ the percentage of intergranular fracture went up to 85% as shown in Figure 4.19. The percentage of intergranular fracture at no applied current was approximately 10%. the percentage of intergranular fracture as a function of applied cathodic current is plotted in Figure 4.20. In the 90-10 copper nickel samples fatigued with applied cathodic current, the amount of intergranular fracture appears to vary linearly with the amount of applied current.

Fractographic observations were also made on the surfaces of the failed copper nickel fatigue specimens. Some slip band formation was observed on the surfaces perpendicular to the fracture surface, but the predominant feature present was secondary cracking as seen in Figures 4.21 and 4.22. This secondary cracking was intergranular and appeared to increase in severity as the applied cathodic current was increased. The fracture

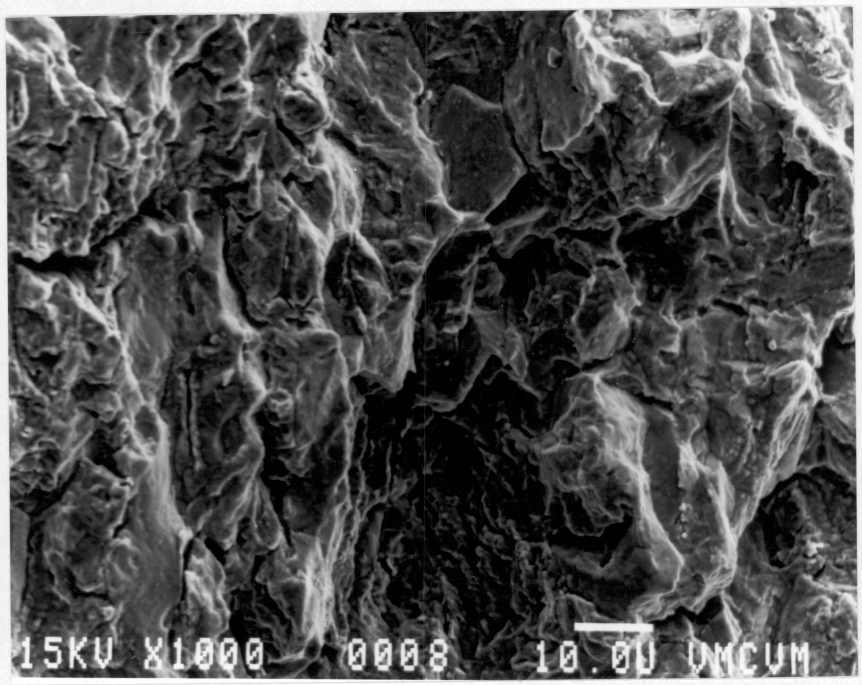

Figure 4.18 Stage II Fatigue crack propagation region for sample tested at 331 $\mu A/cm^2$, cathodic (35% brittle fracture).

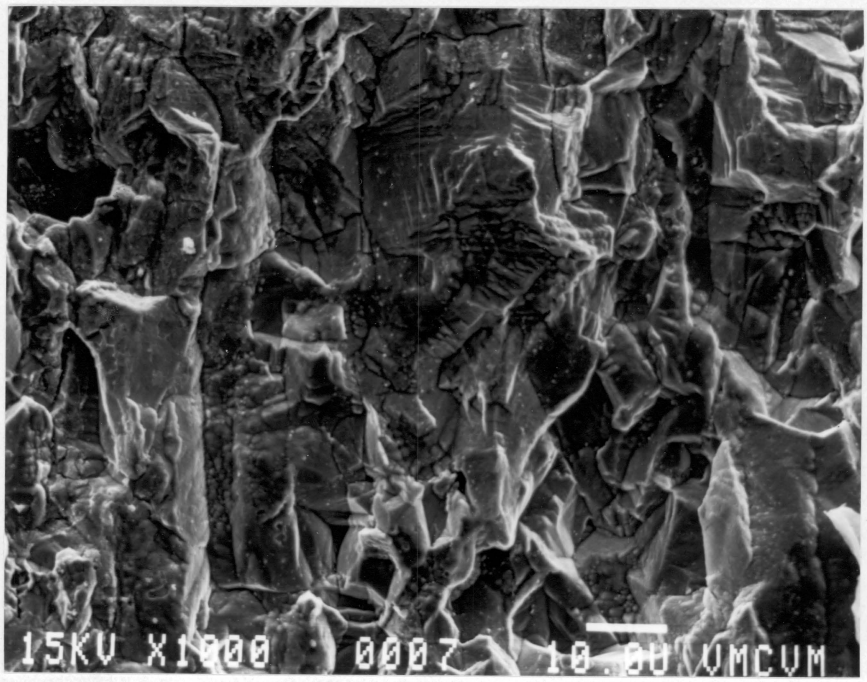

Figure 4.19 Stage II Fatigue crack propagation region for sample tested at 956 $\mu A/cm^2$, cathodic (85% brittle fracture).

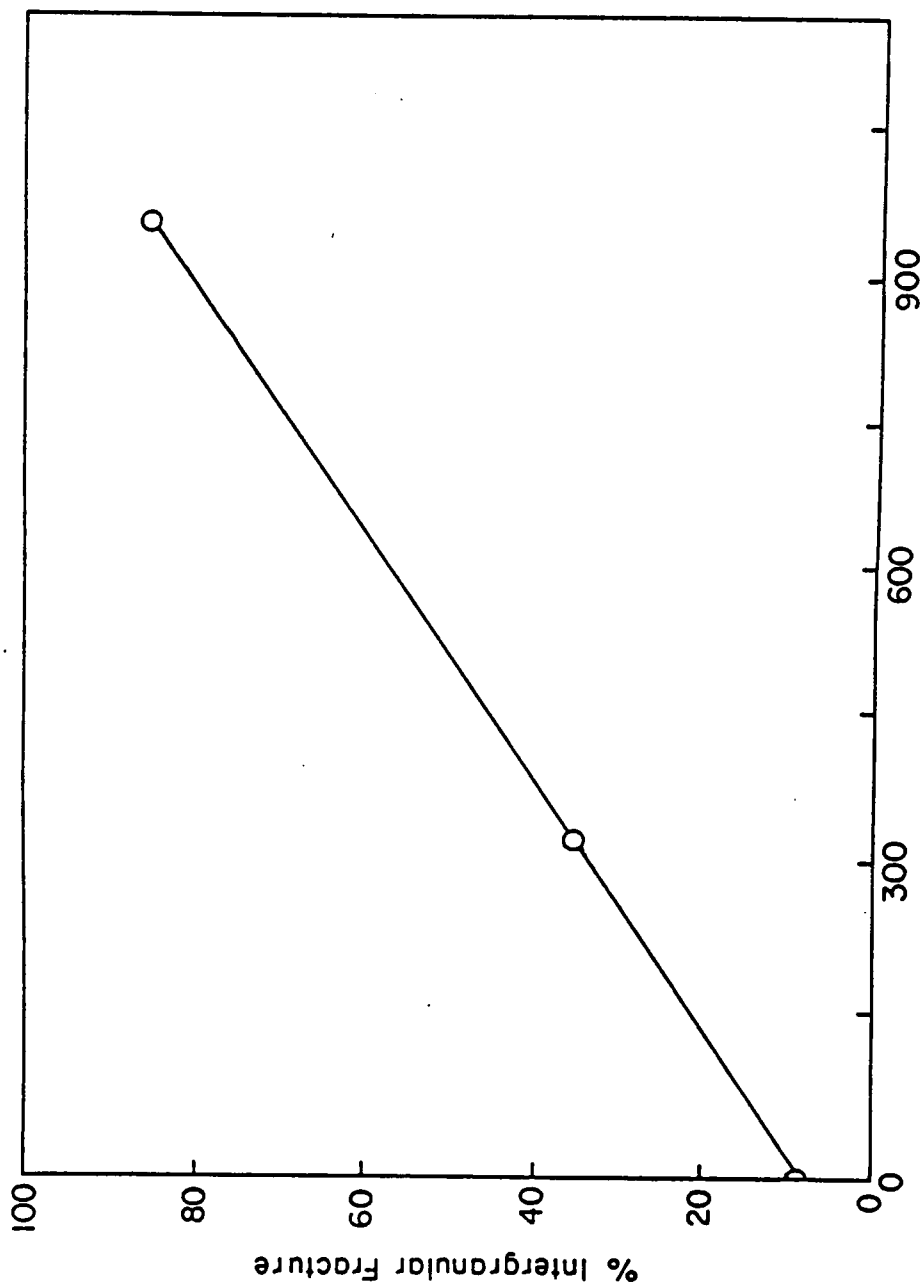

Figure 4.20 Percentage of intergranular fracture as a function of applied cathodic current.

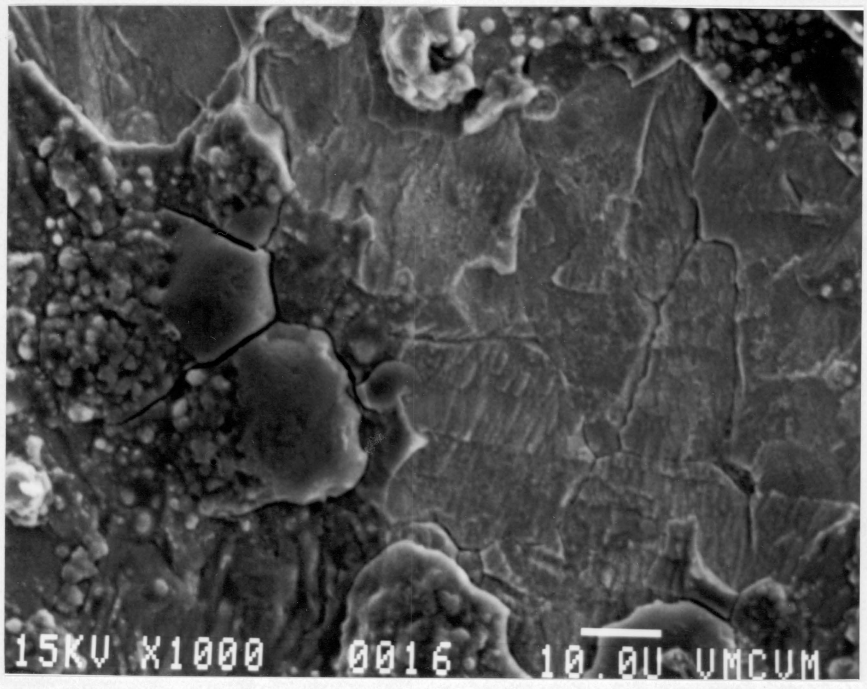

Figure 4.21 Slip bands and secondary intergranular cracking observed on sample tested at 331 $\mu A/cm^2$, cathodic.

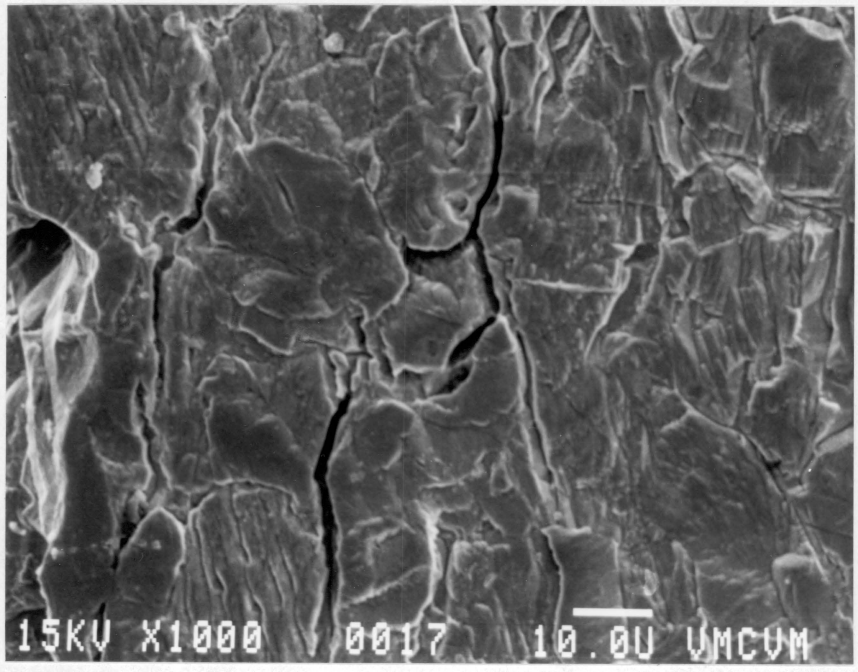

Figure 4.22 Slip bands and secondary intergranular cracking observed on sample tested at 956 $\mu A/cm^2$, cathodic.

mode in the overload region of the samples tested at 331 $\mu A/cm^2$ of cathodic current was ductile rupture as seen in Figure 4.23. In the sample tested at 956 $\mu A/cm^2$ cathodic current, the overload region has some evidence of ductile rupture; however, most of the dimples observed are rather shallow which indicates a shear tearing fracture mode in the overload region of this sample. Figure 4.24 gives an example of the observed fracture surface.

Monotonic Constant Extension Rate Tests

The results of the CERT tests show that the application of a cathodic current increased the time to failure an average of 4.75% over that at no applied current. Correspondingly, the application of an anodic current decreased the time to failure by an average of 1.85%. Also, at every current level, the time to failure at a pH of 1.0 was an average of 1.33% lower than the time to failure at a pH of 6.7 with the greatest difference being at an applied cathodic current of 200 $\mu A/cm^2$. The results of these tests are given in Figure 4.25.

Fractographic analysis of the failed specimens showed that in all of the specimens, regardless of test environment, the dominant fracture mode for both crack initiation and propagation was ductile rupture.

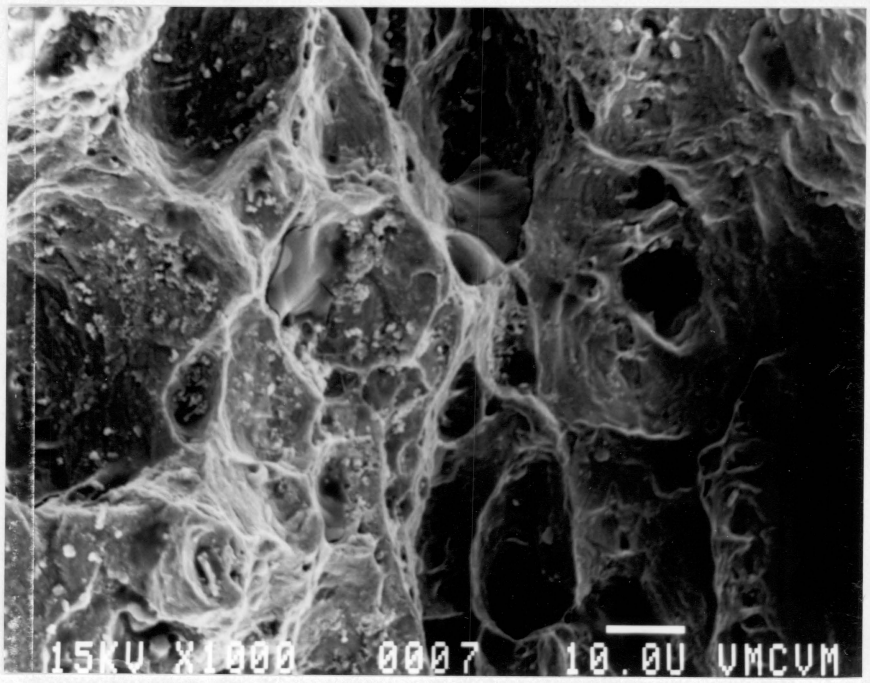

Figure 4.23 Overload region for sample tested at 331 $\mu A/cm^2$, cathodic.

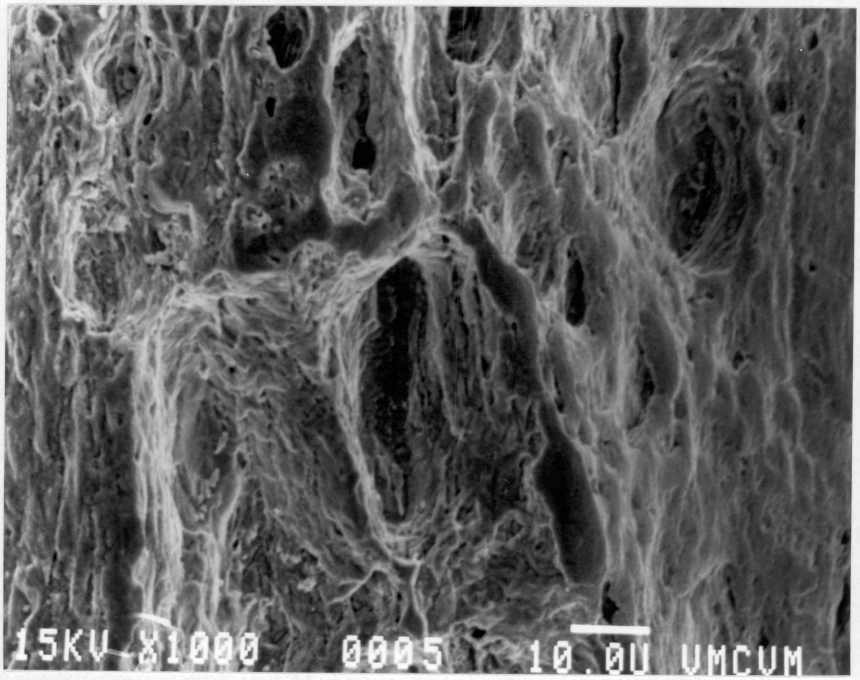

Figure 4.24 Overload region for sample tested at 965 $\mu A/cm^2$, cathodic.

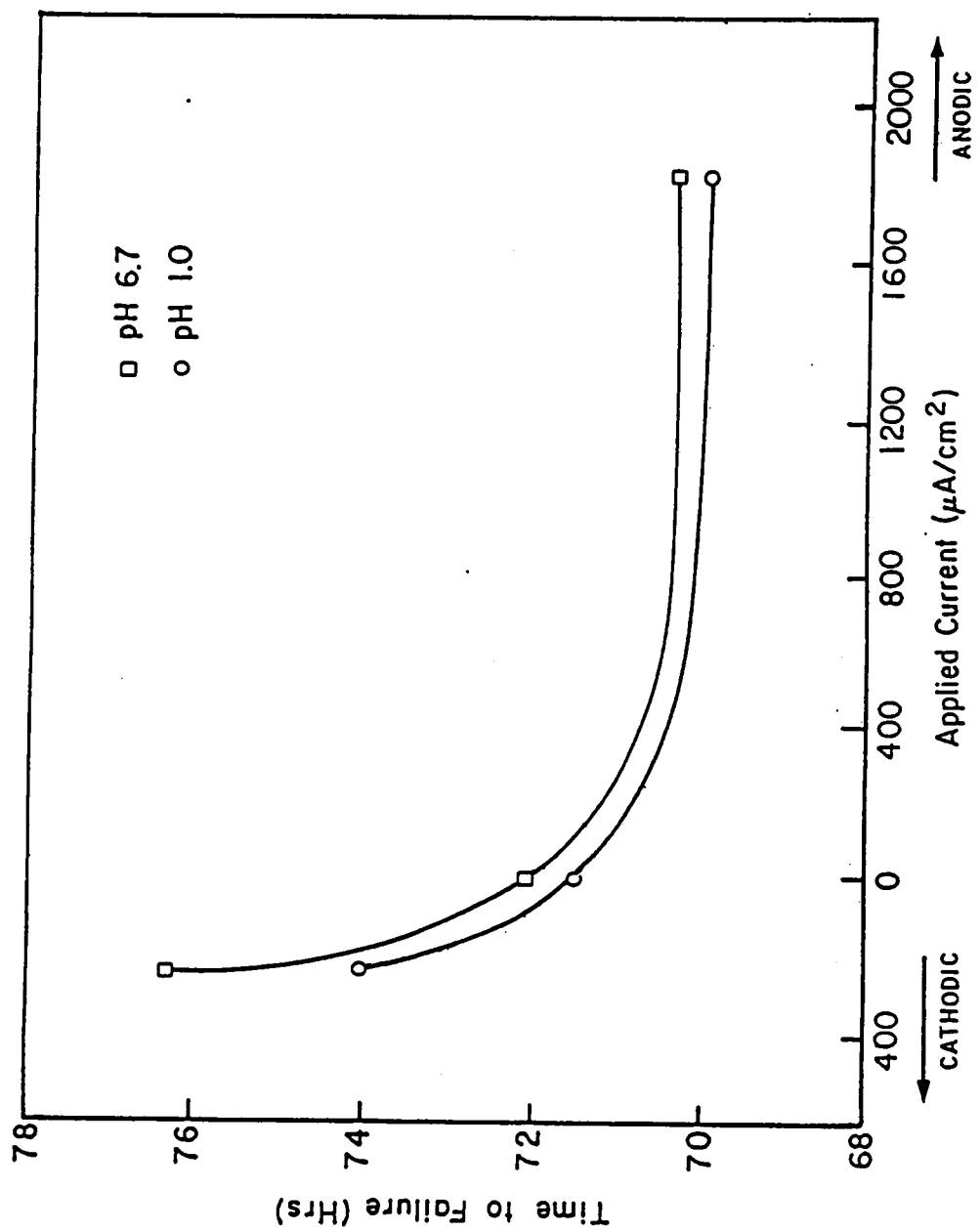

Figure 4.25 Results of constant extension rate tests.

Representative initiation regions for the monotonically tested copper nickel specimens are shown in Figures 4.26 and 4.27. Figures 4.28 and 4.29 show typical crack propagation regions for the samples failed in the CERT tests.

Polarization Studies

The results of the polarization studies conducted to determine the effect of welding on the corrosion behavior of 90-10 copper nickel show that an area with different corrosion characteristics is created by welding. This region corresponds to the heat affected zone of the sample. The polarization curves for the heat affected zone and the 90-10 copper nickel base metal are presented in Figure 4.30. As evident from Figure 4.30, when a given voltage is applied to the welded sample, the heat affected zone has a lower corrosion rate than the base metal. This observation was borne out by the nature of the corrosion products of the two areas. The corrosion product of the heat affected zone was yellow, corresponding to the low anodic current corrosion product found in the fatigue tests while the corrosion product of the base metal was blackish, similar to the high anodic current corrosion product from the fatigue tests.

The investigations of the effect of pH on the corrosion characteristics of 90-10 copper nickel showed

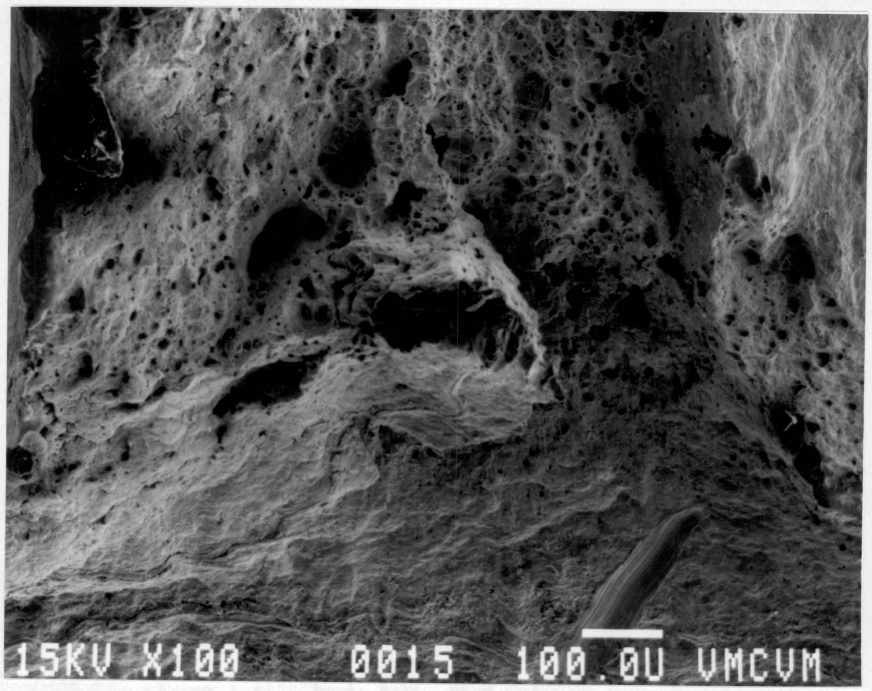

Figure 4.26 Initiation region for CERT sample tested at pH = 6.7 and 200 $\mu A/cm^2$, cathodic.

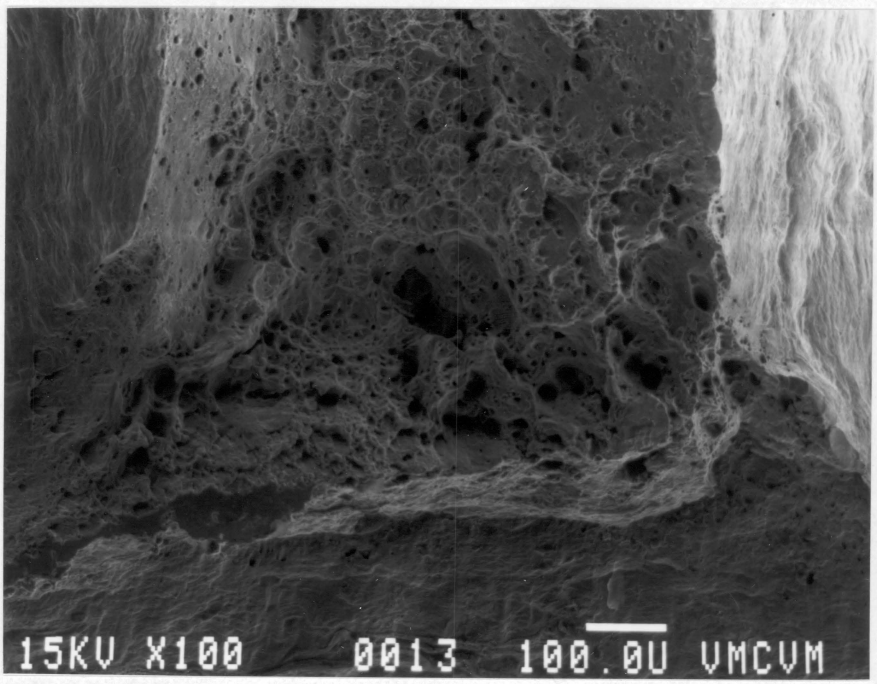

Figure 4.27 Initiation region for CERT sample tested at pH = 1.0 and 1810 $\mu A/cm^2$, anodic.

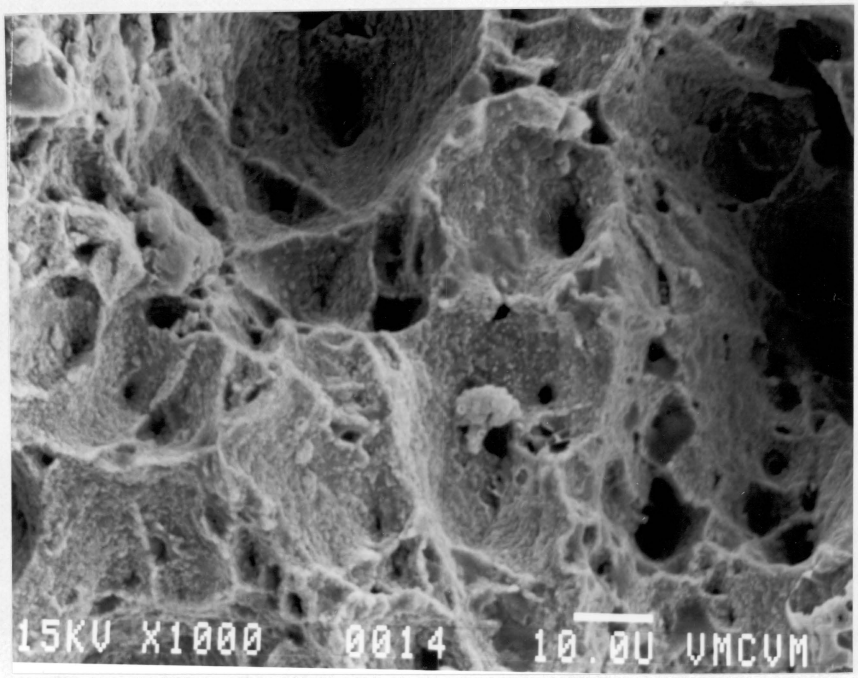

Figure 4.28 Propagation region for CERT sample tested at pH 6.7 and 200 $\mu A/cm^2$, cathodic.

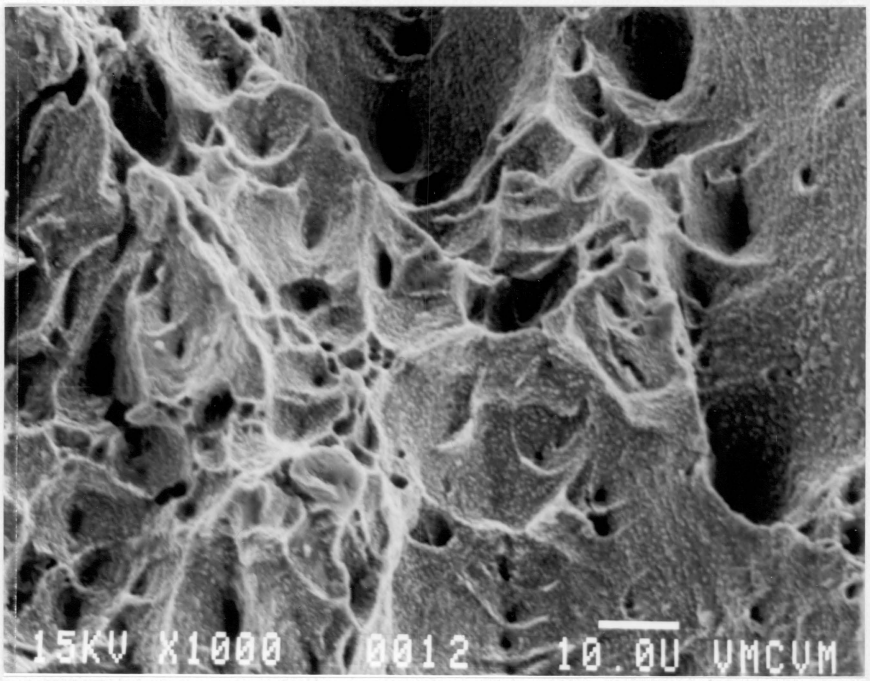

Figure 4.29 Propagation region for CERT sample tested at pH = 1.0 and 1810 $\mu A/cm^2$, anodic.

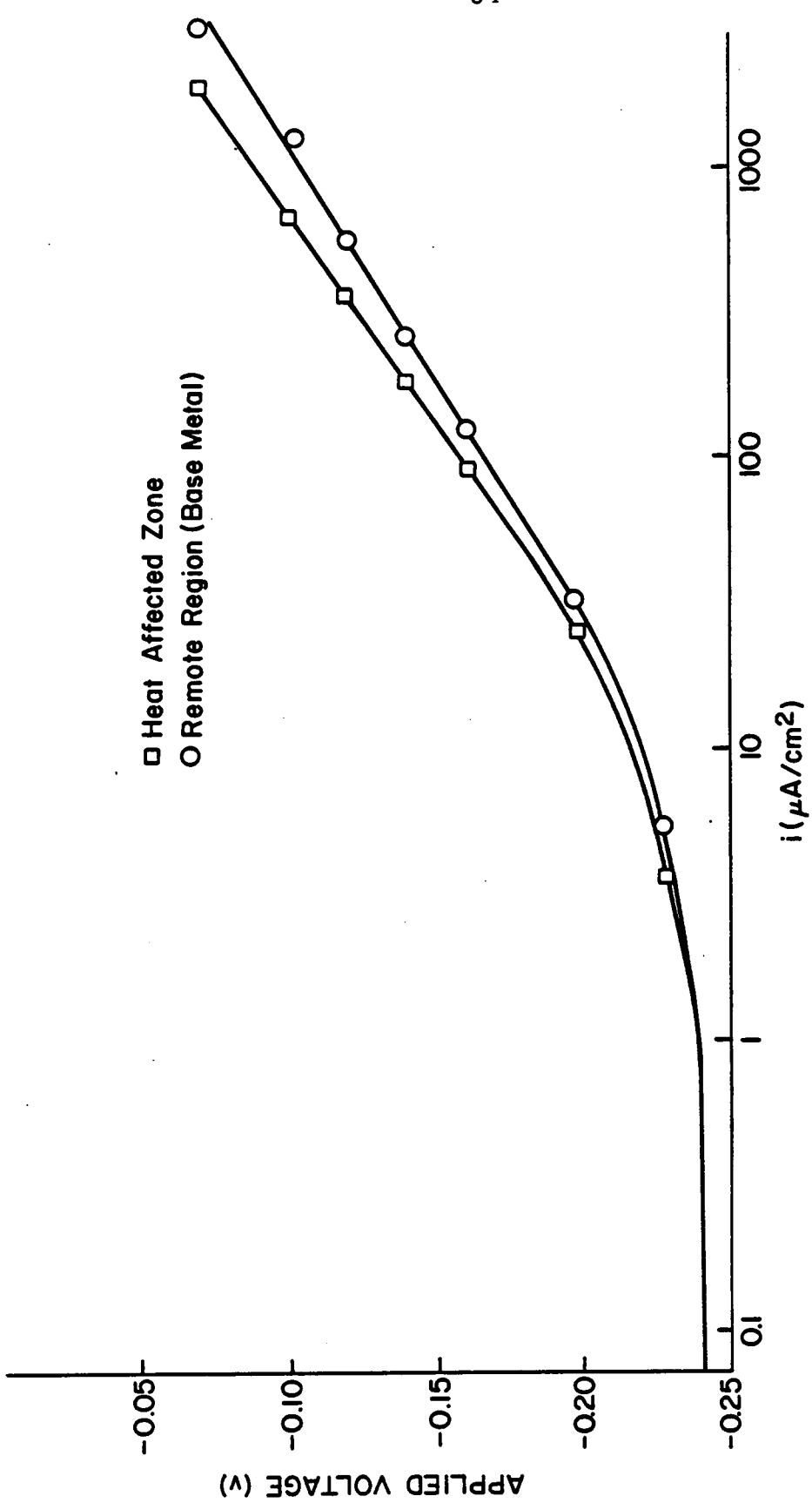

Figure 4.30 Polarization curves for heat affected zone and base metal in welded 90-10 copper nickel specimen.

that the pH of the aqueous environment has a marked effect on the corrosion behavior. The polarization curves for a sample of 90-10 copper nickel in the three solutions of differing pH are shown in Figure 4.31. From these curves, it is apparent that as the pH of the aqueous environment is lowered, the corrosion rate of 90-10 copper nickel increases for any applied potential. The pH of the aqueous environment also effects the passivation of the 90-10 copper nickel. At a pH of 6.6, the copper nickel specimen began passivation at anodic current less than 100 $\mu A/cm^2$. At a pH of 3.0, the copper nickel began passivation at a current greater than 1000 $\mu A/cm^2$ after an initial breakdown of the protective film. At a pH of 1.0, passivation was not observed to occur.

The results of the studies on the effect of pH on the passivation and film formation of 90-10 copper nickel are shown in Figure 4.32. One observation from this study is that as the initial pH is lowered, the current at which visible film formation occurs is increased. At initial pH's of 9.0 and 11.0 a visible protective film was observed to form with no applied current. At a pH of 6.7 (neutral 3.5% NaCl solution) film formation occurred at 100 $\mu A/cm^2$. at a pH of 3.0, film formation occurred at around 1160 $\mu A/cm^2$ and at a pH of 2.0, at 4560 $\mu A/cm^2$.

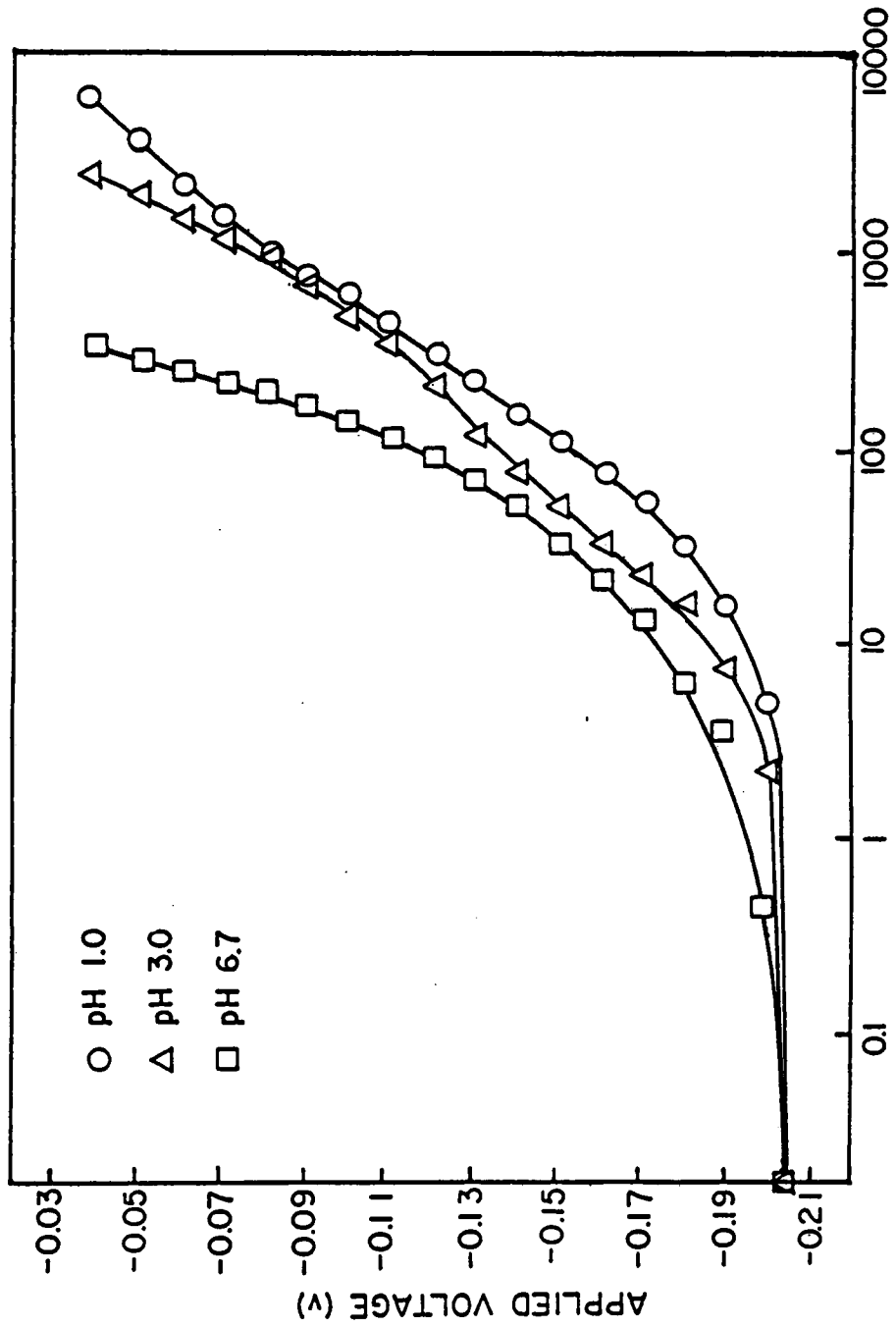

Figure 4.31 Effect of pH on polarization of 90-10 copper-nickel.

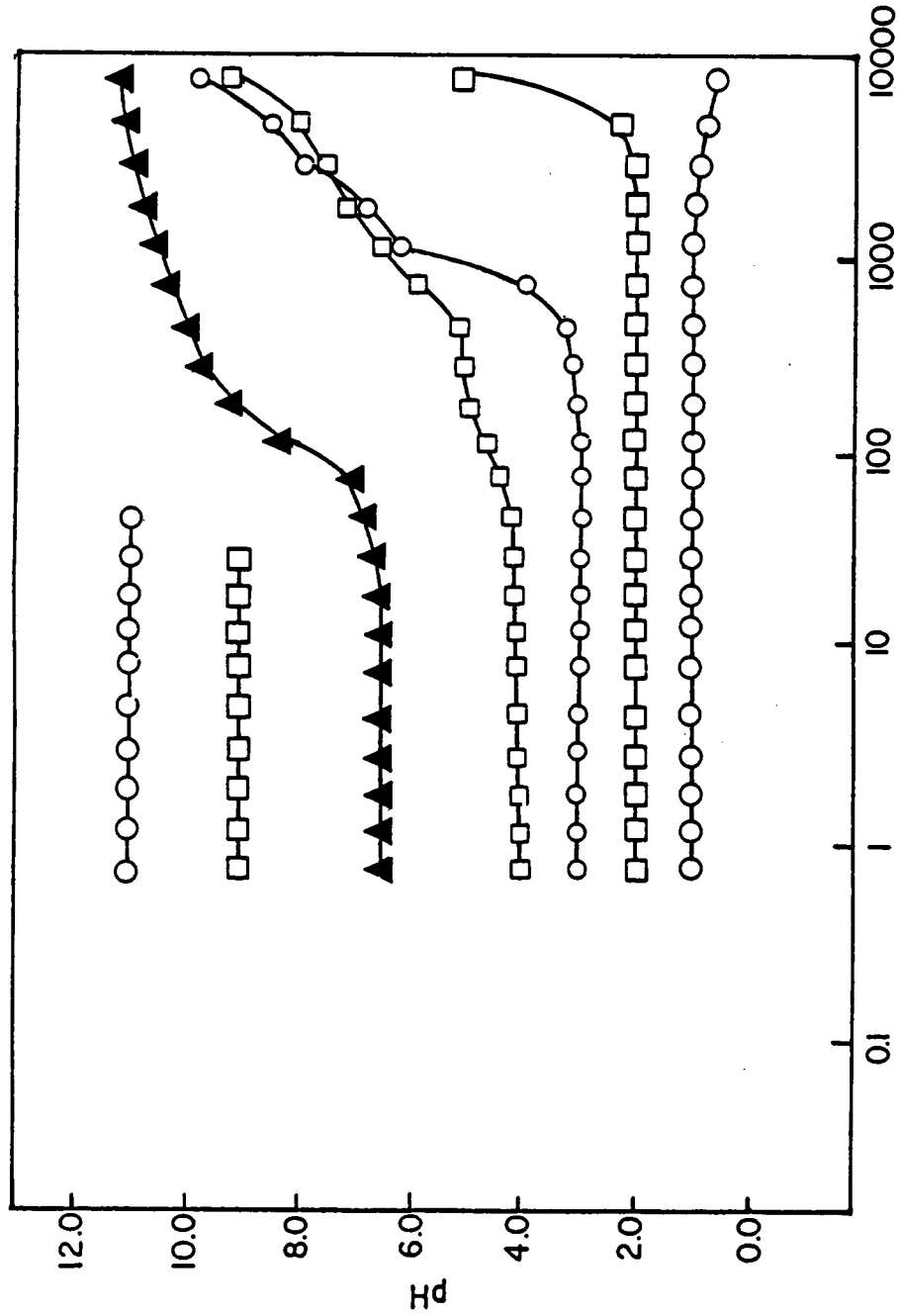

Figure 4.32 Effect of pH on film formation of 90-10 copper-nickel

No film formation occured at a pH of 1.0. At initial pH's of 2.0, 3.0, 4.0 and 6.7, the point of which film formation occurred was accompanied by a sharp rise in the pH of the solution. No such rises were observed for initial pH's of 1.0, 9.0 and 11.0. At pH's of 9.0 and 11.0, complete passivation of the copper nickel specimen occurred.

DISCUSSION

The observed decrease in the corrosion fatigue life of 90-10 copper nickel with an increase of applied anodic current is consistent with observations made in studies involving the corrosion fatigue of other copper-based alloys (22-24, 50). This, along with the observation that applied cathodic currents increase the corrosion fatigue life of 90-10 copper-nickel, suggests that an anodic dissolution process is responsible for the environmentally enhanced fatigue of 90-10 copper nickel in 3.5% NaCl solution at the free corrosion potential.

The results of the constant extension rate tests suggest that the fatigue mechanism in a true corrosion fatigue process (i.e. synergism between corrosive attack and cyclic loading) rather than a stress corrosion fatigue process because the 90-10 copper nickel plates used in this study showed no susceptibility to stress corrosion cracking. Analysis of the fractographic and ESCA data from the fatigue tests with applied anodic current give further insight into the nature of the corrosion fatigue process. As the applied anodic current was increased from zero to 1810 $\mu A/cm^2$, a transition in the fracture mode in both the initiation and propagation regions of the fracture surface was observed. At low

applied anodic currents, the fracture mode was predominantly transgranular while at higher applied currents, an intergranular fracture mode developed. This change is fracture mode in also consistent with observations made from the corrosion fatigue studies of other copper-based alloys (23, 24, 50). In pure copper and in a copper-nickel-chromium alloy (23, 24), this transition to an intergranular fracture mode is rationalized either through a consideration of interactions between mobile dislocations and the environment or through preferential dissolution of emerging slip bands. However, in copper alloys with a second phase which is subject to preferential corrosive attack, such as a duplex aluminum bronze alloy (50), the transition to an intergranular fracture mode with increasing anodic currents was due to the increased corrosive attack at an aluminum rich phase. This intergranular fracture in the aluminum bronze was observed mostly in the interphase regions between the grains of the copper-rich phase and the aluminum-rich phase. This could be due to the increased galvanic effects in the regions. A similar argument may be applied to the increase in intergranular fracture observed in 90-10 copper-nickel. Second phase particles which are iron-rich lie along the boundaries between the copper α-phase grains. These particles

were seen through fractographic studies and in the EDAX scans for chemical analysis. Because iron is a more active species than either copper or nickel, preferential corrosion of the iron rich second phase particles should be expected. This preferential removal of material along the grain boundaries leads to stress concentrations in these areas and therefore shifts the fracture path to the grain boundaries. Also, because the Pillings-Bedworth ratio of iron and its oxides are greater than one, it may be surmised that corrosion product wedging adds to the stress present in the grain boundary region and therefore further diverts the fracture path to an intergranular mode. Other observations which suggest that the preferential dissolution of the iron-rich second phase particles occurs were from the ESCA analyses of the corrosion products collected from the fatigue tests and from the change in color of the corrosion products during fatigue. At no applied current, there is four times as much iron as copper in the corrosion product. Also, there is a significant amount of chloride in the corrosion product. From this information, plus the fact that the corrosion product was yellow, it can be surmised that the major component of the corrosion product was $FeCl_2$. As the applied anodic current is increased to 181 $\mu A/cm^2$, the iron to copper ratio in the corrosion

product increases to over thirteen. The corrosion product darkened to an orange color and the percentage of chloride ions in the corrosion product decreased, but was still detectable. This information indicates that while $FeCl_2$ was still present, another iron corrosion product was also present. Fe_2O_3 or one of its hydrates is a likely candidate because of its reddish-brown color. This combined with $FeCl_2$ can give the orange color which was observed.

As the applied anodic current was increased past 181 $\mu A/cm^2$, several changes in the corrosion fatigue behavior of the 90-10 copper nickel were observed. First of all, the nature of the corrosion product changed. The iron to copper ratio dropped back down to a value of less than four at 330 $\mu A/cm^2$ and asymptotically approached zero as the current was increased even further. This was reflected in further changes in the color of the corrosion product. The corrosion product changed to progressively darker shades of brown and chloride ions were no longer detected. A likely candidate for the copper corrosion products is $CuO_2 \cdot H_2O$. This particular oxide of copper is brown to brownish black which explains the increasing darkness of the corrosion product as the percentage of copper increases. At the two highest current levels (1810 $\mu A/cm^2$ and 18,100 $\mu A/cm^2$), nickel

was also detected in the corrosion product. Nickel oxide is a black corrosion product. This black product also corresponds to the observed color at high current levels. The fatigue life drops off sharply with an increase in applied anodic current from zero to about 150 to 200 $\mu A/cm^2$. After that point, the fatigue life drops off more gradually. A similar behavior is observed in the percent intergranular fracture as a function of applied current curve. At the lower levels of applied anodic current, the percentage of intergranular fracture increases faster than at the higher levels of applied current. These changes in the nature of the corrosion product, the rate of decline in fatigue life and rate of increase in intergranular fracture corresponds to the anodic current levels where film formation and passivation begins. Therefore, it is very likely that a change in the corrosion fatigue mechanism of 90-10 copper nickel is occurring and that the mechanism makes a transition from localized dissolution to surface film rupture. A surface film rupture mechanism at higher applied anodic currents would explain the decrease in rates of change in fatigue life and percent intergranular fracture. Since repassivation is occurring at the crack tip to some degree, this repassivation would decrease the effect that a given increase in applied anodic current

compared to the no film situation. This was demonstrated in the tests of the effect of pH on the polarization of 90-10 copper nickel. At a pH of 6.7, film formation occurred and consequently the corrosion rate was lower than at a pH of 1.0 where no film formation was observed.

When the applied cathodic current was increased, the fatigue life of 90-10 copper nickel was increased. However, a substantial increase in the percentage of intergranular fracture also occurred with the increase in cathodic current. Furthermore, with applied cathodic current,secondary cracking along grain boundaries was observed on the surfaces of the 90-10 copper nickel perpendicular to the fracture surface. These two observations suggest that hydrogen embrittlement may be occurring along the grain boundaries and that although lower levels of cathodic current are beneficial to the corrosion fatigue behavior of 90-10 copper nickel because the current inhibits anodic dissolution, high levels of applied cathodic current may induce decreases in the fatigue life of 90-10 copper nickel. Observations of this sort were made in corrosion fatigue studies involving mild steels (70, 80) where low levels of cathodic current were beneficial but high levels of cathodic current were detrimental because of hydrogen embrittlement.

From the experimental results, evidence for three different corrosion fatigue mechanisms was obtained. The occurrance of a given mechanism depends on the applied current. If the applied current is such that the copper-nickel specimen is in the active region of the polarization curve, a preferential dissolution mechanism involving second phase iron particles is dominant. If the copper nickel is in the passive region, a surface film rupture mechanism is operative. In the immune region, 90-10 copper nickel can be susceptible to hydrogen assisted fatigue crack growth. This sort of behavior suggests that the Process Competition Model for fatigue crack growth is most appropriate for decribing the corrosion fatigue behavior of 90-10 copper nickel.

There was some difference but not an extremely large difference between the times to failure in the constant extension rate tests. There were also no effects of either pH or applied current of the fracture mode in monotonic failure. These results indicate that no synergistic effects between monotonic loading and corrosion occur in 90-10 copper nickel plates. All of the differences in time to failure can be related solely to corrosion rates. At both pH 6.7 and pH 1.0, the samples with an appied anodic current failed faster than those sample with no applied current which in turn failed

faster than those samples with an applied cathodic current. These small differences in monotonic testing reflected larger differences that were observed in fatigue testing. At all current levels, the samples tested at pH 1.0 failed faster than those tested at pH 6.7 due to the retardation of film formation at the lower pH. It can be argued that as the small differences in time to failure due to applied current in the CERT tests reflected large differences in fatigue testing, the small differences in time to failure due to pH in the CERT tests would indicate that the pH level of an environment will greatly influence the corrosion fatigue behavior of 90-10 copper nickel.

The results of the polarization studies on the welded copper nickel sample showed that the near weld region or heat affected zone corroded at a lower rate than the base metal remote from the weld. This lower corrosion rate in the heat affected zone could be due to changes in the metallurgical structure of the copper nickel due to the welding process. Changes could include dissolution of the iron particles. However, because the iron particles are known to precipitate at room temperature, this explanation is not very likely. Alternatively, the lower corrosion rate in the near weld region could be due to galvanic effects because the

copper nickel is in direct contact with the Monel weld. Whatever the reason, the welding process appears to be beneficial in terms of the corrosion fatigue behavior of 90-10 copper nickel.

CONCLUSIONS

The results of this study have shown that the corrosion fatigue behavior of 90-10 copper nickel is strongly dependent upon the environment to which it is exposed. Applied anodic currents decrease and applied cathodic currents increase the corrosion fatigue life of 90-10 copper nickel. The application of both anodic and cathodic currents caused a change in the fatigue fracture mode from predominantly transgranular to intergranular. As the applied anodic current was increased, the composition of the corrosion product changed. At low currents the major metallic element in the corrosion product was iron while at higher anodic currents, copper was the predominant metallic element. Also, at higher applied anodic currents, the amount of decrease in life for a given increase in applied current was lower than the decrease in life seen at lower current levels. In monotonic loading, the environment had very little effect on the failure of 90-10 copper nickel. Polarization studies showed that the pH of the environment affects the corrosion rate and film formation of 90-10 copper nickel. Welding causes the creation of a heat affected zone which has different corrosion characteristics than those of the 90-10 copper nickel base metal. From these results, the

following conclusions may be drawn.

1. In 90-10 copper nickel, there are three different corrosion fatigue mechanisms corresponding to the three different regions of the polarization curve. These three mechanisms are:
   a. preferential dissolution of iron-rich second phase particles in the active region,
   b. surface film rupture in the passive region and
   c. surface energy reduction due to adsorption of hydrogen in the immune region.
2. These three processes appear to be competitive and at free corrosion potential, the mechanism of preferential dissolution of iron particles is dominant.
3. These plates of 90-10 copper nickel show no susceptibility to stress corrosion cracking, therefore the corrosion fatigue mechanism must be true corrosion fatigue.
4. In terms of structural integrity of 90-10 copper nickel plates attached to steel marine structures, the best conditions to keep the cladding in is that of cathodic protection since the longest corrosion fatigue lives were observed when a cathodic current was applied.

5. Welding seems to be beneficial to the corrosion fatigue behavior of 90-10 copper nickel because it results in the lowering of the corrosion rate at the near weld regions.

REFERENCES

1. J. M. Popplewell, R. J. Hart and J. A. Ford; Corrosion Science, 1973, 13, p. 295.

2. W. C. Stewart and F. L. LaQue; Corrosion, 1952, 8, p. 259.

3. M. Prager, L. K. Keay and E. W. Thiele, Jr.; Welding Journal, 1978, 9.

4. S. M. Fisher, D. Fiederick, M. R. Louthan, Jr. and J. H.Wilson; Welding Journal, 1983, 14, p. 37.

5. H. E. Frankel, J. A. Bennett and W. A. Pennington; Trans. ASM, 1960, 52, p. 257.

6. P.H. Frith; J. Iron Steel Inst., 1948, 159, p. 385.

7. W. A. Wood; Fatigue in Aircraft Structures, Academic Press, New York, 1956.

8. A. N. May, Nature, 1960, 185, p. 303.

9. T. H. Lin and Y. M. Ito, J. Mech. Phys. Solids, 1969, 17, p. 511.

10. P. Neumann, Acta Met., 1969, 17, p. 219.

11. A. H. Cottrell and D. Hull, Proc. Roy. Soc., A242, 1957, 211.

12. D. J. McAdam, Jr. and G. W. Geil, Proc. ASTM 41, 1941, 696.

13. B. B. Wescott, Mech. Eng., 1938, 60, p. 813.

14. M. T. Simnad and U. R. Evans, Proc. Roy. Soc., A188, 1947, p. 372.

15. D. J. Duquette and H. H. Uhlig, Trans. ASM, 1968, 61, p. 449.

16. C. Laird and D. J.Duquette, Corrosion Fatigue: Chemistry, Mechanics and Microstructure, NACE 2, 1972, p. 88.

17. D. J. Duquette, Fatigue and Microstructure, ASM, Metals Park, Ohio, 1979, p. 335.

18. R. N. Parkins, Corrosion Fatigue, The Metals Society, London, 1983, p. 36.

19. A. J. Gould and U. R. Evans, J. Iron and Steel Inst., 1947, 156, p. 531.

20. D. J.Duquette and H. H. Uhlig, Trans. ASM, 1969, 62, p. 839.

21. D. Whitwham and U. R. Evans, J. Iron and Steel Inst., 1950, 165, p. 72.

22. H. N. Hahn and D. J. Duquette, Met. Trans., 1979 10A.

23. H. N. Hahn and D. J.Duquette, Acta Met., 1978, 26, p. 279.

24. H. Masuda and D. J.Duquette, Met. Trans., 1975, 6A.

25. S. P. Lynch, Mechanisms of Environment Sensitive Cracking of Materials, The Metals Society, London, 1977, p. 201.

26. R. E. Stoltz and R. M. Pelloux, Met. Trans., 1972, 3, p. 2433.

27. L. Montgrain and P. R. Swann, Hydrogen in Metals, 1977, Paris, p. 575.

28. P. J. E. Forsyth and D. A. Ryder, Metallurgica, 1961, 63, p. 117.

29. J. Weertman, Mech. of Fatigue, ASME, 1981, p. 11.

30. P. Neumann, Acta Met., 1974, 22, p. 155.

31. C. Laird and G. C. Smith, Phil. Mag., 1962, 7, p. 849.

32. C. Q. Bowles and D. Broek, Int. J. of Frac. Mech., 1972, 8, p. 75

33. M. Kikukawa, M. Jono and M. Adachi, Fatigue Mechanisms, ASTM STP 675, 1979, p. 234.

34. P. Neumann, H. Fuhlrott and H. Vehoff, Fatigue Mechanisms, ASTM STP 675, 1979, p. 371.

35. H. W. Liu, Mechanics of Fatigue, ASME, 1981, p. 53.

36. B. Tomkins and W. D. Biggs, J. of Matl. Sci., 1969, 4, p. 544.

37. R. J. H. Wanhill, Met. Trans., 1975, 6A, p. 1587.

38. R. van der Welden, H. L. Ewalds, W. A. Schultze and A. Punter, Corrosion Fatige: Mechanics, Metallurgy, Electrochemistry and Engineering, ASTM 801, 1983, p. 64.

39. K. Endo, K. Komai and T. Shikida, ibid., p. 81.

40. E. P. Dahlberg, Trans. ASM, 1965, 58, p. 46.

41. W. A. van der Sluys, J. Basic Eng., 1965, 87, p. 363

42. R. P. Wei and J. P. Landes, Mater. Res. Std., 1969, 9, p. 25.

43. J. P. Gallagher and J. M. Sinclair, J. Basic Eng., 1969, 91, p. 598.

44. M. J. Horden, Acta Met., 1966, 14, p. 1173.

45. R. P. Wei, Int. J. Frac. Mech., 1968, 4, p. 159.

46. J. A. Feeney, J. C. McMillan and R. P. Wei, Met. Trans., 1970, 1, p. 1741.

47. D. E. Piper, S. H. Smith and R. V. Carter, Metals Eng. Quar., 1968, 8, p. 50.

48. D. A. Meyn, Rept. NRL Progress, Nove. 1968, p. 20.

49. T. R. Shives and J. A. Bennett, J. Matl. Sci., 1968, 3, p. 695.

50. P. Collins and D. J.Duquette, Corrosion, 1978, 34, p. 119.

51. T. Pyle, V. Rollins and D. Howard, Corrosion Fatigue: Chemistry, Mechanics and Microstructure, NACE, Houston, 1971, p. 312.

52. V. Rollins, C. Patel and T. Pyle, I. Mech. E. Conf. Publ. 1977-4, London, 1977, p. 367.

53. P. J. E.Forsyth, Acta Met., 1963, 11, p. 703.

54. T. Pyle, V. Rollins and D. Howard, J. Electrochem. Soc., 1975, 122, p. 1445.

55. C. Patel, T. Pyle and V. Rolins, Met. Sci., 1977, 11, p. 185.

56. C. Patel, T. Pyle and V. Rollins, Nature, 1977, 266, p. 517.

57. F. P. Ford and T. P. Hoar, Proc. of 3rd Int. Conf. on Strengthening of Metals and Alloys, Cambridge, 1973, paper 95.

58. C. Amzallag, P. Rabbe and A. Desestret, Corrosion Fatigue Technology, ASTM STP 642, 1978, p. 117.

59. J. A. Moskovitz and R. M. Pelloux, ibid., p. 133.

60. R. Ebara, T. Kai and K. Inoue, ibid., p. 155.

61. D. A. Jones, Met. Trans., 1985, 16A, p. 1133.

62. L. Montgrain and P. R. Swann, Second Int. Cong. on Hydrogen in Metals, Paris, 1977, p. 575.

63. G. M. Seamans and C. D. S. Tuck, Second Int. Cong. on Hydrogen in Metals, Paris, 1977, paper 4A11.

64. Torronen and M. Kemppainen, Corrosion Fatigue: Mechanics, Metallurgy, Electrochemistry and Mechanics, ASTM STP 801, 1983, p. 287.

65. C. Q. Bowles and J. Schijve, ibid., p. 96.

66. I. M. Austen and P. McIntyre, Metal Science, 1979, 13, p. 420.

67. D. A. Meyn, Met. Trans., 1971, 2, p. 853.

68. R. Holder, I. Mech. E. Conf. Publ. 1977-4, London, 1977, p. 37.

69. H. Doker and D. Munz, ibid., p. 123.

70. T. W. Crooker, F. D. Bogar and W. R. Cares, NRL Report 8042, NRL, Wash. D. C., 1976.

71. O. Vosikousky, Journal of Eng. Mat. and Technology, Oct. 1975, p. 298.

72. C. T. Fujii and J. A. Smith, Corrosion Fatigue: Mechanics, Metallurgy, Electrochemistry and Engineering, ASTM STP 801, 1983, p. 390.

73. I. M. Austen and E. F. Walker, I. Mech. E. Conf. Publ. 1977-4, London, 1977, p. 1.

74. T. Broom and A. Nicholson, J. Inst. Metals, 1960, 89, p. 183.

75. A. Hartmann, Int. J. Frac. Mech., 1965, 1, p. 167.

76. F. J. Bradshaw and C. Wheeler, Appl. Mater. Res., 1966, 5, p. 112.

77. T. W. Crooker, R. W. Judy, Jr., E. A. Lange and R. E. Morey, Trans. ASM, 1966, 59, p. 195.

78. P. J. Trant, I. Mech. E. Conf. Publ. 1977-4, London, 1977, p. 57.

79. H. P. Chu and J. G. Macco, Corrosion Fatigue Technology, ASTM STP 642, 1978, p. 223.

80. R. D. Hibbert and W. D. Dover, I. Mech. E. Conf. Publ. 1977-4, London, 1977, p. 145.

81. T. Hodgkeiss, Mechanisms of Environment Sensitive Cracking of Materials, The Metals Society, London, 1977, p. 348.

82. L. A. Glikman, Corrosion-Mechanical Strength of Metals, Butterworths, London, 1962.

83. J. W. Kochera, J. P. Tralmer and P. W. Marshall, Paper OTC 2604, Offshore Technology Conference, Houston, May 1976.

84. L. P. Pook and A. F. Greenan, Fatigue Testing and Design, Vol. 2, The Soc. of Env. Eng., London, April 1976, p. 30.1.

The 4 page vita has been removed from the scanned document

The 4 page vita has been removed from the scanned document

The 4 page vita has been removed from the scanned document

The 4 page vita has been removed from the scanned document